The Reaction Mechanism Analysis of Enzymes with Degrading Persistent Dyes and its Rational Designs

(難分解性色素分解酵素の反応機構解析とその合理的設計)

Issei Omura

大村 翼世

Graduate School of Chemical Sciences and Engineering

Hokkaido University

北海道大学　大学院総合化学院

2023

ACKNOWLEDGMENTS

I would like to express my sincere thanks to Professor Koichiro Ishimori. In spite of his busy schedule, he not only gave me much advice and discussion on my study, but also encouraged me wholeheartedly in my research life. I am deeply grateful to Associate Professor Takeshi Uchida for his precise advice on my study and constant direction. I am very grateful to thank Professor Tomohide Saio of Tokushima University for his continued kindness and counsel regarding my study and career path after his transfer from Hokkaido University, Secretary Maki Tanaka for accepting office procedure that I could not handle on my own and making delicious coffee every weekday, and the members on Structural Chemistry Laboratory for helps and assistance.

I would like to express my deepest gratitude to my family: my parents who always took care of me living far away from my hometown for 9 years, my brothers and sister who cheered for me in my research life.

Finally, Japan Science and Technology Agency headquarters Spring supported my Ph.D. course.

March, 2023

Graduate School of Chemical Sciences and Engineering,

Hokkaido University

Issei Omura

LIST OF PUBLICATIONS

CHAPTER II

Takeshi Uchida, Issei Omura, Sayaka Umetsu, Koichiro Ishimori “Radical transfer but not heme distal residues is essential for pH dependence of dye-decolorizing activity of peroxidase from *Vibrio cholerae*”, *Journal of Inorganic Biochemistry*, 2021, **219**, 111422

CHAPTER III

Issei Omura, Koichiro Ishimori, Takeshi Uchida “Converting cytochrome *c* into a DyP-like metalloenzyme”, *Dalton Transactions*, 2022, **51**(33) 12641-12649

LIST OF PRESENTATIONS

Oral Presentations

1. Issei Omura, Koichiro Ishimori, and Takeshi Uchida

   "Converting cytochrome *c* into DyP-like metalloenzyme by molecular design"
   The 53rd Symposium on Chemical and Biological Oxidation (Virtual)
   November 7, 2020

2. Issei Omura, Koichiro Ishimori, and Takeshi Uchida

   "Creating an Artificial Dye-Decolorizing Peroxidase Rationally Designed Using Cytochrome *c*"
   The 54th Symposium on Chemical and Biological Oxidation (Virtual)
   October 30, 2021

Poster Presentations

1. Issei Omura, Koichiro Ishimori, and Takeshi Uchida

   "Shifting the optimum pH for the dye-decolorizing activity of Dye-decolorizing peroxidase"
   The 28th Symposium on Role of Metals in Biological Reactions, Biology and Medicine (SRM2018), (Sendai, Japan) June 29, 2018

2. Issei Omura, Koichiro Ishimori, and Takeshi Uchida

   "Elucidation of the mechanism of dye-decolorizing reaction of DyP from *Vibrio cholerae* and the conversion of the optimal pH"
   The 52nd Symposium on Chemical and Biological Oxidation, (Nara, Japan) November 9, 2019

3. Issei Omura, Koichiro Ishimori, and Takeshi Uchida

   "Designing an artificial enzyme like dye-decolorizing peroxidase using cytochrome *c"*
   The 47th Symposium on Biomolecular Science (Virtual) June 4, 2021

4. Issei Omura, Koichiro Ishimori, and Takeshi Uchida

   "Converting cytochrome *c* into a dye-degrading enzyme for. environmental remediation"
   Integrated Bio-metal Science Summer camp (Virtual) September 4, 2021

5. Issei Omura, Koichiro Ishimori, and Takeshi Uchida

   "Improving dye-decolorizing activity of dye-decolorizing peroxidase at neutral pH"
   The International Chemical Congress of Pacific Basin Societies 2021 (Virtual) December 20, 2021

6. Issei Omura, Koichiro Ishimori, and Takeshi Uchida

   "Converting cytochrome *c* into a dye-degrading enzyme for environmental remediation"
   The 1st symposium of Integrated Bio-metal Science (Tokyo, Japan) May 22, 2022

7. Issei Omura, Koichiro Ishimori, and Takeshi Uchida

   “Constructing cytochrome *c* with enhanced dye-decolorizing activity”
   12th International Conference on Porphyrins and Phthalocyanines (ICPP-12) (Madrid, Spain) July 14, 2022

8. Issei Omura, Koichiro Ishimori, and Takeshi Uchida

   “Design and creation of cytochrome *c* having an efficient dye-degrading activity”
   Integrated Bio-metal Science Summer training camp (Rusutsu, Japan) September 4, 2022

9. Issei Omura, Koichiro Ishimori, and Takeshi Uchida

   “Creating artificial enzyme with dye-degrading activity for bioremediation”
   The 55th Symposium on Chemical and Biological Oxidation (Sapporo, Japan) November 5, 2022

10. Issei Omura, Koichiro Ishimori, and Takeshi Uchida

    “Converting Cytochrome *c* into a DyP-like Enzyme”
    10th Asian Biological Inorganic Chemistry Conference (AsBIC-10) (Kobe, Japan) November 30, 2022

CONTENTS

CHAPTER I

General Introduction

1.1 Water pollution by synthetic dyes

Synthetic dyes are widely used in the dyeing industry because of their color stability, ease of availability, and low production cost. Anthraquinone dyes, which are typical synthetic dyes, have multiple aromatic rings to enhance coloration. They are also sulfonated or nitrated to make them more soluble in water and to reduce their degradability. The use of anthraquinone dyes is preferred in the textile industries because of their structural features.

With the development of the textile industry, the use of large amounts of synthetic dyes has become increasingly prevalent, leading to their discharge into the environment. These dyes have complex structures that make them difficult to degrade naturally, raising concerns about their potential impact on ecosystems and human health. Consequently, the treatment of wastewater containing these compounds has become a significant challenge, particularly in developing countries where the textile industry is thriving.

It has been reported that anthraquinone dyes can be removed by various physical and chemical methods, including precipitation, adsorption, filtration, coagulation, oxidation, electrochemical destruction, ozone treatment, and photocatalysis[1]. However, these methods are not economically feasible in terms of overall treatment costs and environmental impact based on the huge volume of effluents.

On the other hand, biological methods using microorganisms and enzymes can remove pollutants under mild conditions and are less expensive and more environmentally friendly than physical and chemical methods. Recently, bacteria and enzymes capable of degrading anthraquinone dyes have been reported[2,3], and their use is expected to reduce environmental pollution caused by synthetic dyes.

1.2 Dye-decolorizing peroxidase

Dye-decolorizing peroxidase (DyP) (EC 1.11.1.19) is an enzyme that easily degrades anthraquinone dyes. This enzyme was isolated from *Geotrichum candidum* (later revised to *Bjerkandera adusta*) and DyPs have been found in many organisms[4]. The dye degradation reaction by DyP has been proposed to convert anthraquinone dyes to less toxic phthalic acid (Figure 1.1)[5]. Also, H_2O_2 used in this reaction is environmentally friendly, as it decomposes into water, and is inexpensive. Therefore, DyP is expected to be used for the purification of effluents containing synthetic dyes, which is discharged from textile factories.

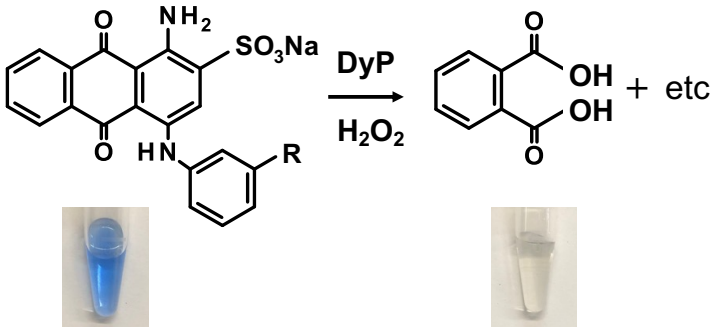

Figure 1.1 The proposed anthraquinone dye degradation scheme by DyP
It is proposed that DyP decomposes anthraquinone dyes with hydrogen peroxide to produces phthalic acid.

DyP usually works under acidic conditions, such as pH 3-4, and its activity is low at the neutral pH. The pH of effluents from textile industry is said to be neutral to alkaline[6], and the optimum pH of rivers is generally near neutral. Therefore, it is necessary to create a mutant DyP with high dye degradation activity at neutral pH.

In this thesis, I worked on the design and creation of artificial DyP with high dye-degrading activity at neutral pH. In addition, to explore environmental remediation methods using the DyP mutant, I investigated ways in which artificial DyP can be used to

degrade anthraquinone dyes. Enzymes may lose their activity when exposed to an environment that differs from physiological conditions. To solve this problem, I investigated the dye-degrading activity of *E. coli* expressing the mutant DyP. The growth rate of *E. coli* is very fast, and proteins can be easily expressed using it. In addition, since *E. coli* grows under neutral conditions, it was thought to be a good match for artificial DyP with dye-degrading activity at neutral pH.

1.3 pH dependence of dye-decolorizing activity of DyP (Chapter II)

Several studies have shown that the dye degradation reaction of DyPs is a mechanism by which radicals generated by the reaction of the heme of DyP with H_2O_2 are transferred to Tyr and Trp on the protein surface to degrade the dye[7–9] . However, the key factor determining the pH dependence of dye-degrading activity is still unknown. In chapter II, I analyzed the dye-degrading activity of DyP based on its crystal structure and reaction mechanism and created an artificial enzyme capable of degrading anthraquinone dyes under neutral pH, using DyP from *Vibrio cholerae* (*Vc*DyP) (Figure 1.2) because the pH dependence of the dye degradation reaction of *Vc*DyP has been proposed[10]. Based on the structure of *Vc*DyP and its reaction mechanism, I tried to create a *Vc*DyP mutant with high dye-degrading activity at neutral pH and investigated the dye degradation activity of *E. coli* expressing this mutant. Through these analyses, I discussed the factor that plays an important role in the pH dependence of the dye degradation reaction of DyP.

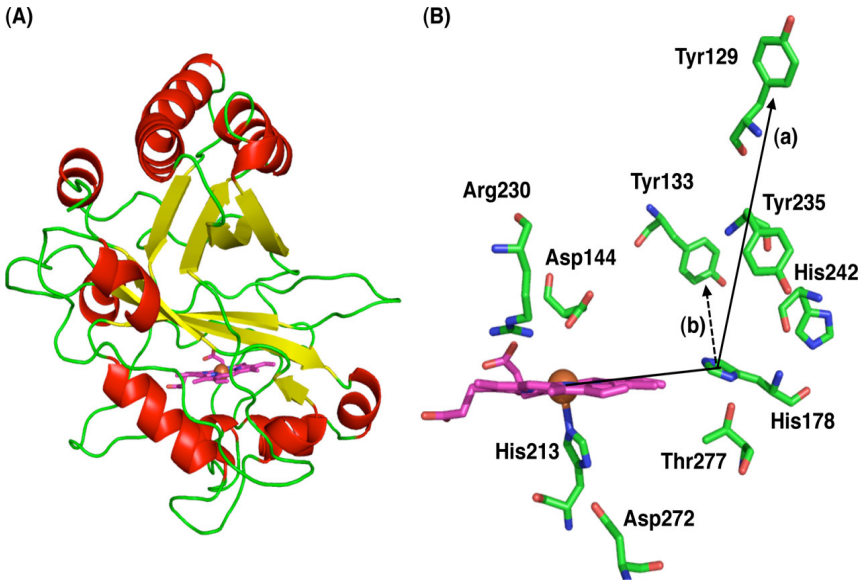

Figure 1.2 Crystal structure of *Vc*DyP (PDB entry 5DE0)[10].
(A) α-Helices and β-strands of a *Vc*DyP subunit are colored red and yellow, respectively. The heme is colored pink. (B) Close-up around the heme-binding site, including the catalytically relevant residues. Putative pH-dependent radical transfer pathway at lower pH (a) and higher pH (b). Copyright 2015, ACS publications[10]

1.4 Converting cytochrome *c* into a DyP-like enzyme (Chapter III)

In chapter II, I succeeded in creating a DyP mutant with dye-degrading activity at neutral pH, but the dye-degrading activity of the *E. coli* expressing it was not as high as expected from enzymatic activity measurements. One of the reasons for the low activity was thought to be that DyP expressed in *E. coli* does not generate radicals, which are essential for dye-degrading activity, because heme is not bound to DyP. To solve this problem, I focused on cyt *c*, which forms a covalent bond with heme in cells (Figure 1.3). Cyt *c* plays a role in electron transfer in the respiratory chain. Cyt *c* has been also reported that the dissociation of the axial ligand Met 80 from heme iron increases the reactivity of heme with H_2O_2[11,12]. In chapter III, I tried to create an artificial enzyme that can degrade persistent dyes using cyt *c* and examined the dye-degrading activity of *E. coli* expressing

this enzyme. Based on the structure of DyP and the reaction mechanism of dye degradation, I introduced mutations in cyt *c* using several approaches and examined the design of mutants with high activity.

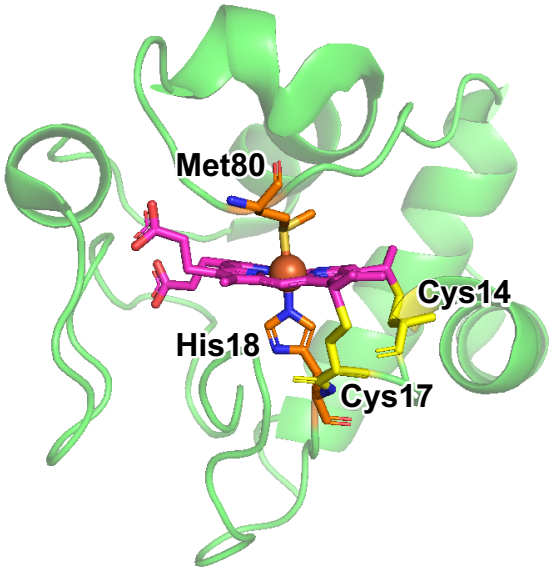

Figure 1.3 Crystal structure of cyt *c* (PDB ID: 6K9I). Heme is covalently atached to this protein.

References

1. Lade, H., Govindwar, S. & Paul, D. Mineralization and detoxification of the carcinogenic azo dye Congo red and real textile effluent by a polyurethane foam immobilized microbial consortium in an upflow column bioreactor. Int. J. Environ. Res. Public. Health., **12**, 6894–6918 (2015).
2. Kim, S. J. & Shoda, M. Decolorization of molasses and a dye by a newly isolated strain of the fungus Geotrichum candidum Dec 1. Biotechnol. Bioeng., **62**, 114–119 (1999).
3. Banat, I. M., Nigam, P., Singh, D. & Marchant, R. Microbial decolorization of textile-dyecontaining effluents: A review. Bioresour Technol **58**, 217–227 (1996).
4. Sugano, Y. & Yoshida, T. DyP-Type Peroxidases: Recent Advances and Perspectives. Int. J. Mol. Sci., **22**, 5556 (2021).
5. Sugano, Y., Matsushima, Y., Tsuchiya, K., Aoki, H., Hirai, M. & Shoda, M. Degradation pathway of an anthraquinone dye catalyzed by a unique peroxidase DyP from Thanatephorus cucumeris Dec 1. Biodegradation, **20**, 433–440 (2009).
6. Dey, S. & Islam, A. A Review on Textile Wastewater Characterization in Bangladesh. Resources and Environment, **5**, 15–44 (2015).
7. Shrestha, R., Chen, X., Ramyar, K., Hayati, Z., Carlson, E., Bossmann, S., Song, L., Geisbrecht, B. & Li, P. Identification of surface-Exposed protein radicals and a substrate oxidation site in a-Class dye-Decolorizing peroxidase from thermomonospora curvata. ACS Catal., **6**, 8036–8047 (2016).
8. Linde, D. Pogni, R., Cañellas, M., Lucas, F., Guallar, V., Baratto, M., Sinicropi, A., Sáez-Jiménez, V., Coscolin, C., Romero, A., Medrano, F., Ruiz-Dueñ;as, F. & Martínez, A. Catalytic surface radical in dye-decolorizing peroxidase: A computational, spectroscopic and site-directed mutagenesis study. Biochem. J., **466**, 253–262 (2015).
9. Linde, D., Ruiz-Dueñas, F., Fernández-Fueyo, E, Gualler, V., Hammel, K., Pogni, R., & Martínez, A. Basidiomycete DyPs: Genomic diversity, structural–functional aspects, reaction mechanism and environmental significance. Arch. Biochem. Biophys., **574**, 66–74 (2015).
10. Uchida, T., Sasaki, M., Tanaka, Y. & Ishimori, K. A Dye-Decolorizing Peroxidase from Vibrio cholerae. Biochemistry, **54**, 6610–6621 (2015).
11. Sinibaldi, F., Fiorucci, L., Patriarca, A., Lauceri, R., Ferri, T., Coletta, M. & Santucci, R. Insights into cytochrome c-cardiolipin interaction. Role played by ionic strength. Biochemistry, **47**, 6928–6935 (2008).

12. Belikova, N., Vladimirov, Y., Osipov, A., Kapralov, A., Tyurin, V., Potapovich, M., Basova, L., Peterson, J., Kurnikov, I. & Kagan, V. Peroxidase activity and structural transitions of cytochrome c bound to cardiolipin-containing membranes. Biochemistry, **45**, 4998–5009 (2006).

CHAPTER II

Shifting the optimum pH of the dye-degrading activity of DyP

Abstract

In this Chapter, I present the study on the construction of *Vc*DyP mutants that have the maximum dye-degrading activity at neutral conditions. In the mutational studies, it is revealed that the distal Asp, which plays a key role in the peroxidase activity of DyP as acid-base catalyst, does not contribute to the pH-dependence of dye-decolorizing activity of DyP. Based on the crystal structure of *Vc*DyP, I estimated that His178, located near the heme, formed a hydrogen bond to Asp138 and this hydrogen bond contributes to pH-dependent dye-decolorizing activity through inducing alterations in the radical transfer pathway. In order to prevent forming the hydrogen bond, I replaced Asp138 with replaced with Val. The optimal pH for dye-degrading activity of this mutant *Vc*DyP was shifted to pH 6.5. These results indicate that the hydrogen bond between Asp138 and His178 plays an important role in the pH dependence of the dye degradation reaction of *Vc*DyP, and that perturbation of this hydrogen bond can lead to convert the optimum pH of the activity of *Vc*DyP from acidic to neutral pH.

2.1 Introduction

The catalytic degradation property of persistent dyes such as anthraquinone dyes supports the potential biotechnological application of DyPs. However, its low optimal pH is not suitable for practical use.

Two residues (Asp and Arg) in the heme distal pocket are conserved in all DyPs[1–3]. Recent studies have reported that distal aspartic acid or arginine works as catalytic bases during the formation of compound I[4–6]. Although there is no direct evidence to show how and where substrates bind to it, the heme binding pocket is not considered the active site of the dye-degrading reaction, in view of the lack of space for bulky dye compounds near the heme[7–11]. Several studies also have shown that aromatic residues such as tryptophan and tyrosine were located on the protein surface and accumulate and retain radicals[7–9,12]. These data indicate that radicals generated in the reaction with H_2O_2 are transferred to tryptophan or tyrosine on the protein surface, where the dye-decolorizing reaction occurs.

In this chapter, to create mutant *Vc*DyP whose optimum pH of dye-degrading activity is under neutral conditions, I investigated the key factor of the pH dependence of dye-decolorizing activity using DyP from *Vibrio cholerae*. I conducted the research using two approaches. First approach is the introduction of a distal His as an acid-base catalyst since distal residues in the heme binding site are a possible determinant. The second approach is to fix the radical transfer pathway in the dye-degrading reaction. His178 is essential for dye decolorization of *Vc*DyP[7]. I constructed the mutants according to each approach and analyzed dye-degradation activities and investigated the dye-degrading activity of *E. coli* expressing the mutant *Vc*DyP.

2.2 Experimental Procedures

Materials

All chemicals were purchased from Wako Pure Chemical Industries (Osaka, Japan), Nacalai Tesque (Kyoto, Japan), Kanto Chemical (Tokyo, Japan) or Sigma-Aldrich (St. Louis, MO, USA), and used without further purification.

Protein expression and preparation

DyP proteins were expressed and purified as described previously[7]. Briefly, DyP-containing plasmid with the His_6-tag was expressed in *Escherichia coli* BL21(DE3) cells in M9 minimal medium supplemented with 50 μg mL^{-1} kanamycin to suppress the amount of protein-bound protoporphyrin IX. The protein was isolated using HisTrap HP column chromatography (GE Healthcare, Uppsala, Sweden). After reconstitution of protein with an equimolar amount of heme (1:1), the sample was applied to a gel filtration column (HiLoad 16/60 Superdex 200 pg; GE Healthcare) equilibrated with 50 mM Tris-HCl and 150 mM NaCl (pH 8.0). Purity was confirmed via SDS-PAGE as >90%.

Site-directed mutagenesis

Mutagenesis was conducted utilizing the PrimeSTAR mutagenesis basal kit from Takara Bio (Otsu, Japan) using WT expression vector as the template. DNA oligonucleotides were purchased from Eurofins Genomics (Tokyo, Japan). Primers used for construction of mutants are listed in Table 2.1. Genes were sequenced (Eurofins Genomics) to ensure that only the desired mutations were introduced.

Table 2.1: Oligonucleotides used for construction of expression vectors for mutants. The underlined bases signify the introduced mutations.

Mutants	Primers (top, sense; bottom, anti-sense)
D138V	5′–GCACGTGTGATGACGGGCTTTATTGA– 3′
	5′–CGTCATCACACGTGCGTCTAAATAAC– 3′
M139L	5′–ACGTGACCTGACGGGCTTTATTGATG– 3′
	5′–CCGTCAGGTCACGTGCGTCTAAATAAC– 3′
D144H	5′–TTTATTCACGGCACAGAAAACCCGAAAG– 3′
	5′–TGTGCCGTGAATAAAGCCCGTCATGTC– 3′
D144N	5′–CTTTATTAATGGCACAGAAAACCCGA– 3′
	5′–TGTGCCATTAATAAAGCCCGTCATGTC– 3′
H178F	5′–TTTGTGTTCAATTTGCCGGCGTGGAATC– 3′
	5′–CAAATTGAACACAAAGCGTTGTACCATC– 3′
H178W	5′–TTTGTGTGGAATTTGCCGGCGTGGAATC– 3′
	5′–CAAATTCCACACAAAGCGTTGTACCATC– 3′
H178Y	5′–TTTGTGTATAATTTGCCGGCGTGGA– 3′
	5′–CAAATTATACACAAAGCGTTGTACCATC– 3′
L244H	5′–ACGGCCATCTGTTTATTGCGTACTGT– 3′
	5′–TAAACAGATGGCCGTGATCGCCGCTCA– 3′
F246H	5′–CTACTGCATATTGCGTACTGTCACAC– 3′
	5′–CGCAATATGCAGTAGGCCGTGATCGCC– 3′
T278V	5′–CGCTTTGTGAAAGCCGTGACCGGGGCT– 3′
	5′–GGCTTTCACAAAGCGTAGCAGTTGGTC– 3′

Dye-decolorizing assay

Dye-decolorization activity was determined by spectrophotometric measurement of the rate of H_2O_2-mediated decomposition of Reactive blue 19 (RB19). Briefly, 900 µL hemin-reconstituted protein solution (final concentration of 0.3 µM unless specified otherwise) was placed in a 1 mL cuvette along with 10–50 µl substrate solution for testing. The reaction was initiated by the addition of 100 µL of 2 mM H_2O_2 (final conc. 0.2 mM) in the same buffer with incubation for 3 min at 25 °C. The substrate concentration was measured at 595 nm (ε_{595} = 10 mM^{-1} cm^{-1}) using a V-660 spectrophotometer (Jasco, Tokyo, Japan). H_2O_2 concentrations were determined spectrophotometrically using a molar extinction coefficient of 43.6 $M^{-1}cm^{-1}$ at 240 nm[13]. Kinetic parameters (V_{max} and K_M) were assessed by fitting the initial rate (v_0) against substrate concentration ([S]) to the Michaelis-Menten equation as follows:

$$v_0 = \frac{V_{max}[S]}{K_M + [S]} \quad (1)$$

The turnover number (k_{cat}) was obtained by dividing V_{max} by the enzyme concentration.

Peroxidase assay

Peroxidase activity was measured spectrophotometrically. The standard assay was performed in a 2 mL reaction volume containing the enzyme, 0.2 mM H_2O_2 and the appropriate amount of guaiacol (5–150 µM) at 20 °C. The concentrations of the enzyme for guaiacol oxidation assay were 0.3 µM. Reactions were initiated with the addition of H_2O_2 and initial rates for guaiacol oxidation monitored at 470 nm (ε_{470} = 26.6 mM^{-1} cm^{-1})[14]. Data were fitted to the Michaelis-Menten equation.

Electron Transfer Calculation

Possible electron transfer pathways were predicted using the PATHWAY module of the program HARLEM module [15–17] based on coordination from *Vc*DyP crystal structure (PDB code 5DE0)[7]. All calculations were performed using default setting.

Dye-decolorizing assay using *E. coli* overexpressed mutant enzymes

E. coli BL21(DE3) transformed with the pET26b(+) *Vc*DyP vector was incubated in Luria-Bertani (LB) media at 37 ºC under shaking at 200 rpm. 0.2 mM of isopropyl-β-D-1-thiogalactopyranoside (IPTG) and 40 μM RB19 were added when the optical density at 600 nm (OD_{600}) reached 0.6.

After 24 hours of incubation, the supernatant of the culture medium was collected by centrifugation, and the change in absorbance of RB19 in the supernatant was measured using a V-570 spectrophotometer (Jasco, Tokyo, Japan).

2.3 Results

2.3.1 Introduction of histidine into the heme distal pocket

The low pH preference for the enzymatic activity of *Vc*DyP is believed to derive from the presence of distal Asp144 (pK_a 3.9). In order to shift the optimal pH of the dye-decolorizing activity of *Vc*DyP to neutral, Asp144 was replaced with histidine (pK_a 6.0) (D144H). The dye-decolorizing activity of D144H mutant was monitored using Reactive blue 19 (RB19) as a substrate. The time course of absorbance changes at 595 nm in the reaction with hydrogen peroxide (H_2O_2) at pH 4.0 is shown in Figure 2.1. The D144H mutant showed almost no change in absorbance at 595 nm at pH 4.0, indicating a significant loss of enzyme activity. The D144H mutant was also inactivated at pH 7.0. The data suggested that the histidine at position 144 is not an acid-base catalyst at any pH.

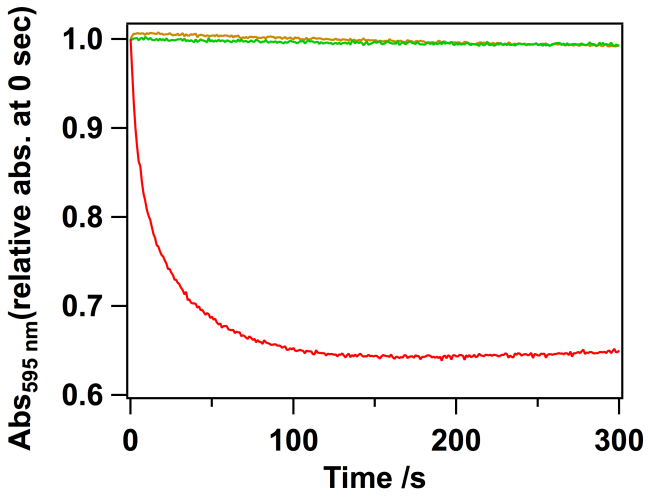

Figure 2.1 Time-course of dye-decolorizing reaction by *Vc*DyP. pH dependence of absorbance changes at 595 nm during catalytic activity of WT at pH 4.0 (black), D144H mutant *Vc*DyP with RB19 at pH 4.0 (ocher), and pH 7.0 (light green).

Previous studies on the peroxidase activity of mutant myoglobin have demonstrated that myoglobin enhanced peroxidase activity when distal histidine was optimally positioned[18,19]. The distance between His144 and heme iron was estimated 4.1 Å (Figure 2.2A), which was the similar value to that of myoglobin (4.0 Å)[20]. This comparison proposed that His144 was located too close to work as acid-base catalyst.

In order to allow distal His to work as acid-base catalyst, I constructed two double mutants, in which His was introduced at a position slightly away from heme iron. In this case, Asp144 was replaced with Val to avoid catalytic competition.

On the basis of the crystal structure of WT *Vc*DyP[7], distances between the heme iron and side-chain of the introduced histidine in each mutant were estimated as 7.2 and 5.4 Å, respectively (Figure 2.2B, C).

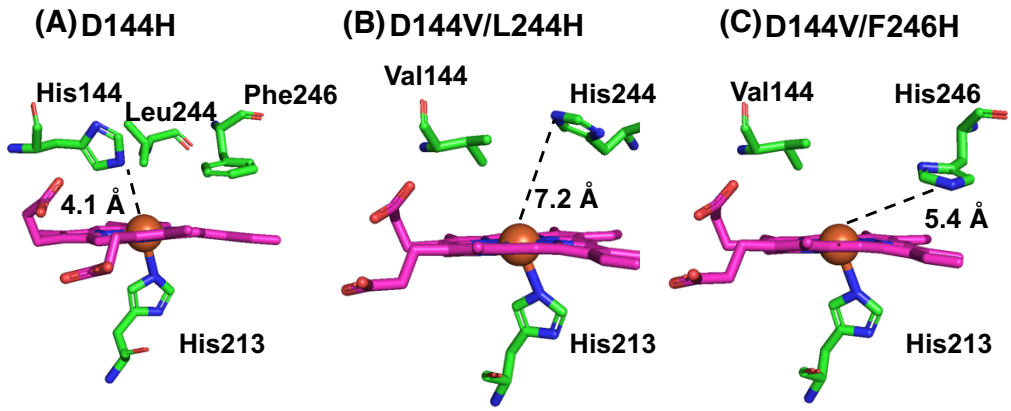

Figure 2.2 Comparison of the heme distal structures of (A) D144H, (B) D144V/L244H, (C) D144V/F246H mutant *Vc*DyP. Model structures were constructed using PyMOL[30].

The time courses of absorbance changes at 595 nm for D144V/L244H and D144V/F246H mutants at pH 4.0 were slower than that of WT *Vc*DyP but significantly faster than that of the D144H mutant (Figure 2.3A). The data exhibited that introduction of histidine at an appropriate position led to restoring of dye decolorization activity.

The pH profiles of the activities of WT, D144V/L244H and D144V/F246H mutant *Vc*DyP were examined (Figure 2.3B) and compared based on the amount of RB19 degraded in the reaction with H_2O_2 at 25 °C for 100 s. For WT *Vc*DyP, activity was highest at pH 4.5 and decreased with increasing pH from 4.5 to 7.0, almost reaching a plateau at pH > 7.0 (Figure 2.3B, black). The pH profile of the D144V/L244H and D144V/F246H mutants showed optimal activity at pH 4.0. The estimated position of His244 in the D144V/L244H mutant appeared to be further from the heme iron (7.2 Å) than the desired range (5–6 Å) (Figure 2.2)[18,21], but the side chain of His 244 may approach the heme iron during the binding of H_2O_2 to heme. As a result, the optimal pH of dye-degrading activity of *Vc*DyP was not shifted to neutral pH by introducing histidine into the heme distal pocket. These results proposed that distal side-chains, such as aspartic acid and histidine, do not contribute to the pH dependence of the dye-decolorizing activity of *Vc*DyP.

In DyP from *Pseudomonas putida*, mutation of distal Asp132 to asparagine led to shifting the optimal pH of dye decolorizing activity from pH 4.3 to 7.4[22]. I expected that replacing Asp144 with Asn would lead to shifting the optimal pH to the neutral condition, and I additionally examined the pH profile of D144N *Vc*DyP (Figure 2.3B, green). However, this mutant was almost inactive over a pH range of 3–10. Collectively, our results support the theory that the distal residues are not involved in determining pH dependence of the dye-decolorizing activity of *Vc*DyP.

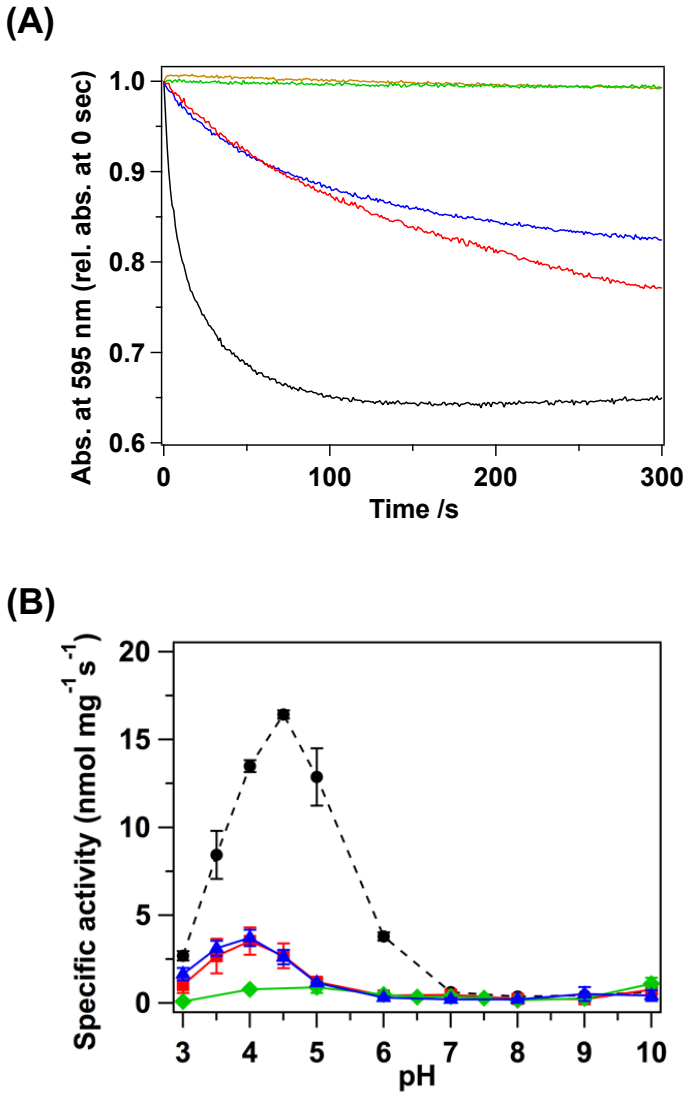

Figure 2.3 (A) Time-course of dye-decolorizing reaction by *Vc*DyP. pH dependence of absorbance changes at 595 nm during catalytic activity of WT at pH 4.0 (black), D144H mutant *Vc*DyP with RB19 at pH 4.0 (ocher), and pH 7.0 (light green), D144V/L244H (blue) and D144V/F246H (red) mutant *Vc*DyP at pH 4.0. The reaction was initiated by the addition of *Vc*DyP (0.3 μM) to RB19 (40 μM) in the presence of H_2O_2 (0.2 mM) at 25 °C. **(B) pH profiles of RB19-decolorizing activities of *Vc*DyPs.** WT (black), D144V/L244H (red), D144V/F246H (blue) and D144N (green) mutant *Vc*DyP. The reaction was initiated by the addition of *Vc*DyP (0.3 μM) to RB19 (40 μM) in the presence of H_2O_2 (0.2 mM) at 25 °C.

2.3.2 pH dependence of compound I formation of *Vc*DyP

As described above, the kind of distal residue in the heme pocket does not contribute to the pH dependence of the dye degradation activity of *Vc*DyP. To examine pH dependence of the reaction with H_2O_2, I investigated the pH profile of the rate of formation of compound I by the reaction of *Vc*DyP with H_2O_2. Firstly, the reactive species in the reaction of *Vc*DyP with H_2O_2 was confirmed. The change of the absorption spectrum of ferric WT *Vc*DyP at pH 7.0 is shown in Figure 2.4A. A Soret band at 405 nm characteristic of the 5-coordinate high-spin heme of *Vc*DyP (Figure 2.4A, black line). Addition of H_2O_2 led to a significant decrease in Soret absorbance, with a concomitant blue shift to 397 nm (Figure 2.4A, red line), accounting for the formation of compound I, as observed for horseradish peroxidase (HRP) and cytochrome *c* peroxidase[23].

Following the addition of o-methoxyphenol (guaiacol), the Soret band gained in intensity to nearly the original level (Figure 2.4A, blue lines), with an increasing broad band at 470 nm from the guaiacol tetramer. A noticeable red shift of the Soret band to 419 nm upon reacting with guaiacol indicated that compound II was formed, as observed in other DyPs[9,24–26]. The pH profile of guaiacol activity exhibited similar to that of dye-degrading activity. For the dye-decolorizing activity, the maximum value at pH 4.5 (16.1 nmol mg^{-1} s^{-1}) was about 30-fold larger than the minimum value at pH 7.0 (0.55 nmol mg^{-1} s^{-1}) (Figure 2.3B). In contrast, the V_0 values for the initial rate with hydrogen peroxide were maximum at pH 4.5 and minimum at pH 7.5, with a maximum V_0 value of 0.60 μM min^{-1} at pH 4.5, 4.6 times larger than the minimum V_0 value (0.13 μM min^{-1}) at pH 7.5 (Figure 2.4B). This data clearly shows that the reaction of *Vc*DyP with H_2O_2 can produce compound I at any pH. Therefore, the pH dependence of the dye degradation activity of *Vc*DyP is not related to the formation of compound I.

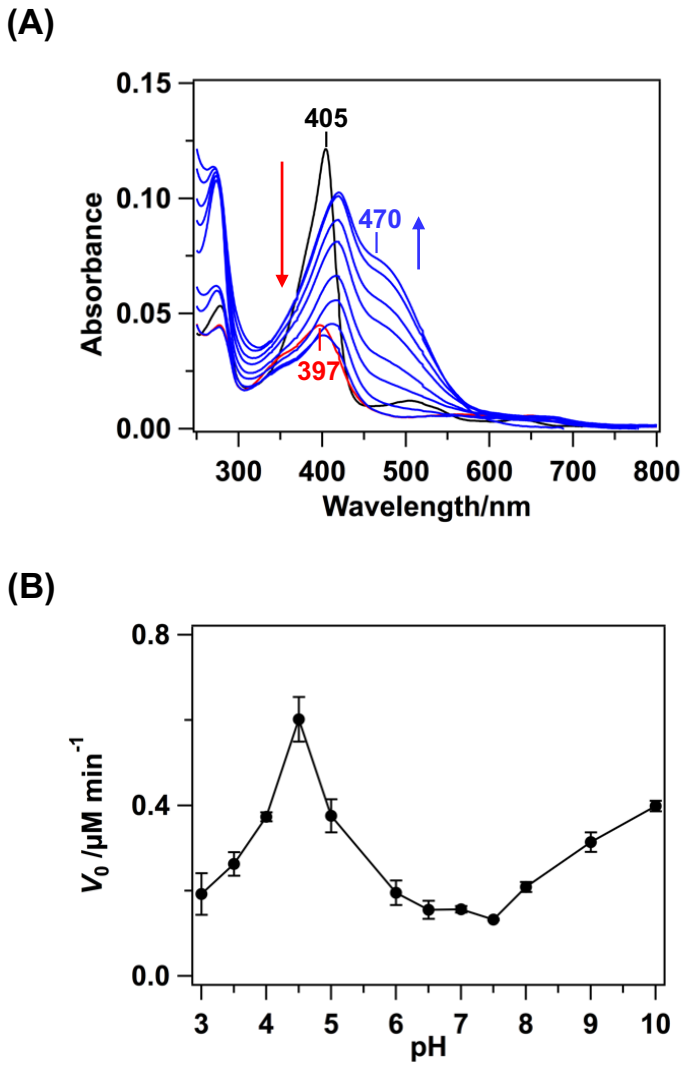

Figure 2.4 Guaiacol oxidation activity of *Vc*DyP. (A) Reaction of *Vc*DyP (0.3 μM) with H_2O_2 (0.2 mM) before (black) and immediately after (red) the addition H_2O_2. Guaiacol (40 μM) was added to H_2O_2-treated *Vc*DyP in 50 mM sodium phosphate (pH 7.0). Spectra were recorded at 4 min intervals for 28 min after the addition of guaiacol (blue). (B) pH profiles of guaiacol activity of WT *Vc*DyP. *Vc*DyP (0.3 μM) was reacted with 40 μM guaiacol and 0.2 mM H_2O_2 at 25°C.

2.3.3 Involvement of His178 in pH-dependent dye-decolorizing activity

In previous studies on the dye-decolorizing activity of DyPs[7–11], the heme pocket is not considered the active site of the dye-decolorizing reaction, in view of the lack of space for bulky dye compounds near the heme. Data from mutational analyses suggest that the active site of dye decolorization including Tyr129 and Tyr235, which are located at a dimer interface ~18 Å apart from the heme iron[7]. For degradation of the bulky substrate, radicals generated by the reaction of heme with H_2O_2 need to be transferred to this location.

Previously, the replacement of His178 located near heme leucine led to losing the dye-decolorizing activity of *Vc*DyP although its guaiacol oxidation activity was similar to that of WT *Vc*DyP. Hence, His178 is proposed as one of the residues that determine the radical transfer pathway from heme to the active site. In order to prevent changing the pH-dependent radical transfer pathway, I constructed three mutants in which His at position 178 was substituted with aromatic residues, such as phenylalanine (H178F), tyrosine (H178Y) and tryptophan (H178W).

The pH profiles of dye-decolorizing activity of the three His178 mutants are shown in Figure 2.5. The pH profile of H178F mutant was similar to that of WT *Vc*DyP. On the other hand, the activities of H178Y and H178W mutants at pH 7 were a slightly higher than that of WT *Vc*DyP despite decreasing the specific activity at pH 3~4. However, considering the experimental errors, these changes were not significant. These results indicated that the presence of an aromatic group such as Tyr or Trp at position 178 facilitates catalytic activity at neutral pH but does not lead to significant improvements of the catalytic activity at neutral pH.

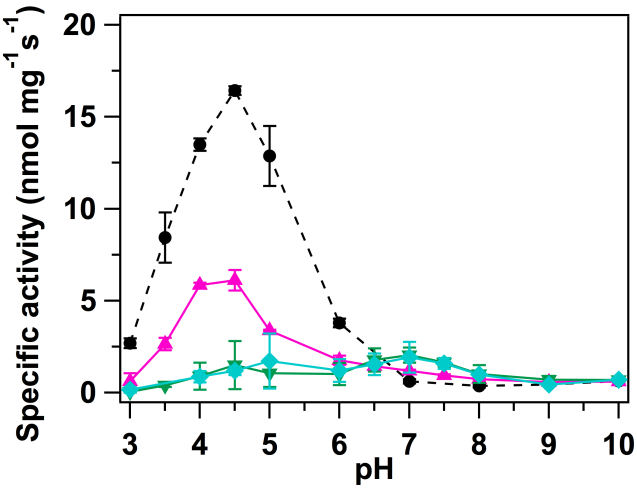

Figure 2.5 pH profiles of RB19-decolorizing activities of *Vc*DyPs. WT (black), H178F (pink), H178W (green), and H178Y (light blue) mutant *Vc*DyP. The reaction was initiated by the addition of *Vc*DyP (0.3 μM) to RB19 (40 μM) in the presence of H_2O_2 (0.2 mM) at 25 °C.

2.3.4 Electron transfer pathway between heme and the active site

Mutant studies on the heme distal residue and His178 of *Vc*DyP suggest that the pH dependence of the dye-decolorizing activity of *Vc*DyP is governed by the radical transfer from heme to the active site, but not the heme distal residue. In a previous study on *Vc*DyP, Tyr129 and Tyr235, located at the dimer interface, are the active site of the dye-decolorizing reaction at acidic pH. On the other hand, at neutral pH, radicals are transferred to Tyr109 and Tyr133, and consumed by the formation of a covalent bond between them. I suggested that inhibition of the radical transfer from heme to Tyr109 and/or Tyr133 leads to enhancement of the dye-decolorizing activity at neutral pH. Thus, I predicted the radical transfer pathway from heme to Tyr109 and/or Tyr133 using PATHWAY analysis. Since *Vc*DyP is a dimeric protein and Tyr109 is in another subunit, the radical could be potentially transferred from heme to Tyr133 and then Tyr109 from a different subunit via a through-space jump. Because Tyr109 is the final destination of

radical transfer, the electron pathway was calculated by defining Tyr109 as an electron donor and heme as an electron acceptor.

The predicted electron transfer pathway from Tyr109 to heme involved Thr108, Arg112, Met139, Thr140, and Asp138 (Figure 2.6). To inhibit the radical transfer to this route, I first mutated Met139 to leucine (M139L) because methionine is a possible radical center. However, the pH profile of RB19 degradation by the M139L mutant showed a similar shape to that of WT *Vc*DyP with the optimal pH of 4.0 (Figure 2.7) and comparable specific activity (15 nmol mg^{-1} s^{-1} at pH 4.0) to that for WT (16 nmol mg^{-1} s^{-1} at pH 4.5). As a result, Met139 did not seem to contribute the pH-dependence of radical transfer.

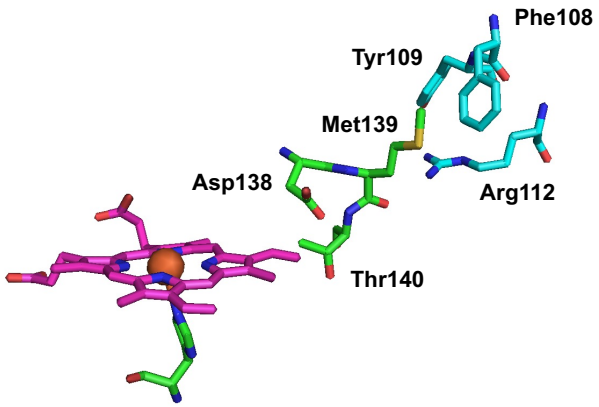

Figure 2.6 Radical transfer pathway from heme to Tyr109 predicted by PATHWAY analysis.

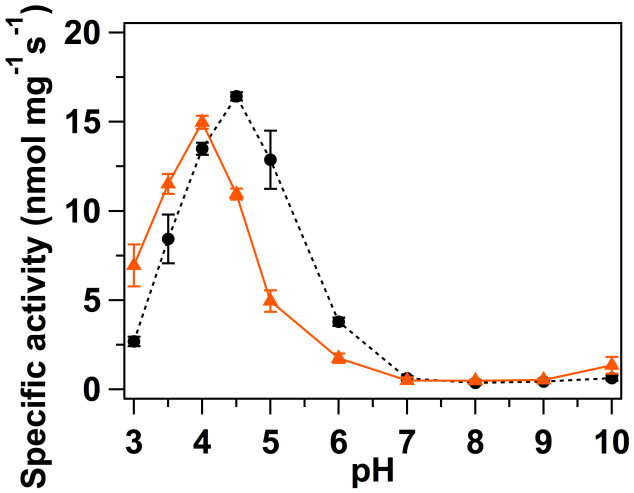

Figure 2.7 pH profiles of RB19-decolorizing activities of *Vc*DyPs. WT (black), M139L (orange) mutant *Vc*DyP. The reaction was initiated by the addition of *Vc*DyP (0.3 μM) to RB19 (40 μM) in the presence of H_2O_2 (0.2 mM) at 25 °C.

2.3.5 Dye-decolorizing activity of D138V and T278V *Vc*DyP

Since the PATHWAY analysis predicted electrons are transferred from Asp138 to heme *via* through-space jump (Figure 2.7), Asp138 is another possible determinant of the pH-dependent DyP activity. Furthermore, the crystal structure of *Vc*DyP showed that His178 is positioned within hydrogen bonding distance of Thr278 (2.9 Å) and Asp138 (3.1 Å) (Figure 2.8). To confirm whether hydrogen bonds of His178 contribute to the pH profile of dye decolorization, I replaced Thr278 or Asp138 with valine (T278V or D138V). Although the maximum specific activity of the T278V mutant was about half that of WT *Vc*DyP, its pH profile for dye decolorizing activity was similar, with maximal activity at pH 4.0–4.5 (Figure 2.9), indicating no shift in the optimal pH value of dye-decolorizing activity. These enzymatic characteristics were similar to those observed for the H178F mutant (Figure 2.5).

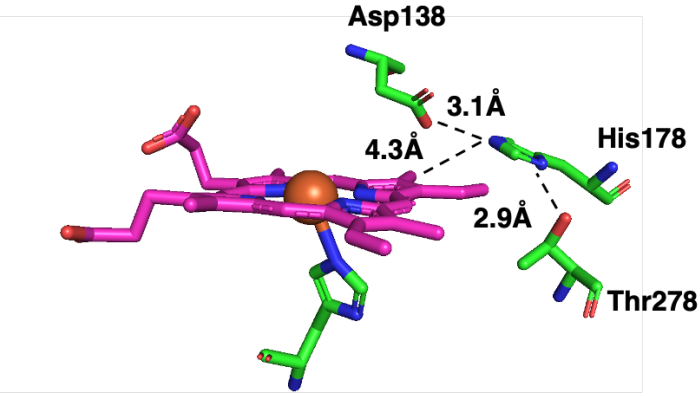

Figure 2.8 Location of Asp138, His178, and Thr278 in *Vc*DyP (PDB 5DE0). Predicted hydrogen bonds are presented in the dotted line.

The pH profile of dye-decolorizing activity of the D138V mutant is shown in Figure 2.9. Although the specific activity of this mutant at pH 3–5 was significantly lower than that of WT enzyme, maximal activity was observed at pH 6.5. Lower activity at acidic pH may be partly due to partial denaturation during measurements. The specific activity of the D138V mutant at pH 6.5 was 5.2 nmol mg^{-1} s^{-1}, which was approximately a third that of WT enzyme at pH 4.5.

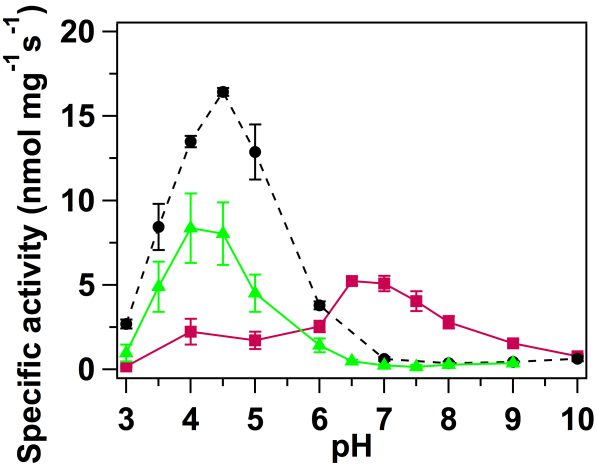

Figure 2.9 pH profiles of RB19-decolorizing activities of WT (black), T278V (light green), and D138V (red) mutant *Vc*DyP. The reaction was initiated by the addition of *Vc*DyP (0.3 μM) to RB19 (40 μM) in the presence of H_2O_2 (0.2 mM) at 25 °C.

2.3.6 pH dependence of compound I formation of D138V *Vc*DyP

To investigate the effect of the substitution Asp138 for Val on reactivity with H_2O_2, I examined the pH profile of guaiacol activity of D138V *Vc*DyP. Interestingly, V_0 of compound I formation was optimal at pH 4.0 (Figure 2.10), suggesting that the radical transfer pathway contributes to the shift in optical pH of the dye-decolorizing activity of the D138V mutant. While His178 forms hydrogen bonds with both Asp138 and Thr278, the results indicate that only the hydrogen bond between His178 and Asp138 is essential for dye-decolorizing activity.

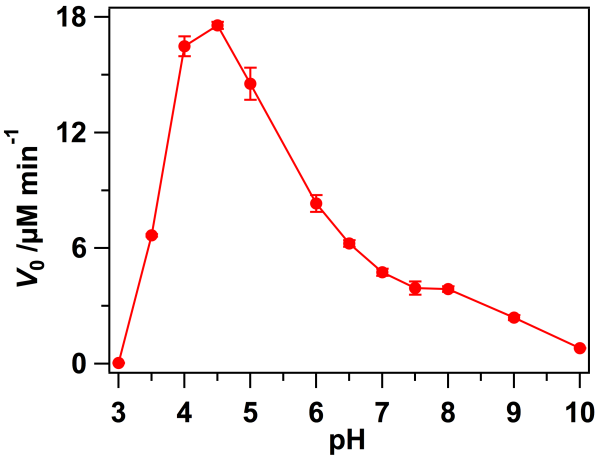

Figure 2.10 pH profiles of guaiacol activity of the D138V mutant *Vc*DyP. *Vc*DyP (0.3 μM) was reacted with 40 μM guaiacol and 0.2 mM H_2O_2 at 25°C.

2.3.7 Whole-cell biocatalyst using *Vc*DyP

I attempted to degrade RB19 using *E. coli*, where *Vc*DyP was overexpressed. wild-type (WT) *Vc*DyP was expressed in the periplasmic space, where substrates are more easily accessible than in the cytoplasm. The *E. coli* was cultured in LB medium with RB19 for 24 hours and the absorbance of the supernatant of the medium was measured. The difference absorbance at 595 nm (ΔAbs 595 nm) was 0.165 (Figure 2.11A). On the other hand, ΔAbs 595 nm in *E. coli* expressing D138V mutant was 0.210 (Figure 2.11B), which was only 1.4-fold higher than in *E. coli* expressing WT *Vc*DyP. In *vitro* experiments showed that the dye-degrading activity of the D138V mutant at pH 6.5 was much higher than that of WT enzyme at neutral conditions. Thus, RB19 was not degraded by the enzyme.

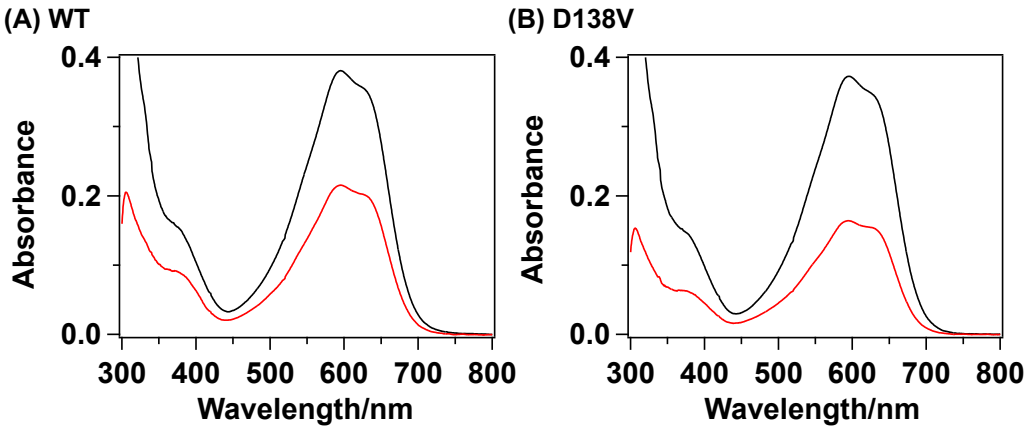

Figure 2.11 Absorbance of the supernatant of culture medium with RB19 (40 μM) of *E. coli* expressed (A) WT and (B) D138V *Vc*DyP; 0h (black line) and 24h (red line).

2.4 Discussion

Effect of distal aspartic acid on pH-dependent dye-decolorizing activity

In a previous study on *Vc*DyP, the substitution of Asp144 with valine led to almost complete loss of dye-decolorization activity[7]. In addition, the optimal pH for the dye-decolorizing activity of *Vc*DyP is pH 4.5. These data indicate that distal aspartic acid is essential for dye decolorization. In contrast, the pH profile of guaiacol oxidation shows that HRP is most active at pH ~6.0, corresponding to the pK_a of the side-chain of histidine[27]. In order to shift the optimal pH to neutral, I substituted Asp144 with histidine. However, this substitution led to the loss of the dye decolorization activity. I also constructed the mutants with a slightly longer distance between N_ε of the distal histidine and heme iron (Figure 2.2B, C) because, like myoglobin[20], the distance in D144H mutant was too short for His144 to work as acid-base catalyst. Although these mutants exhibited the dye-degrading activity, the pH-dependence of the activity was indistinguishable from that of WT *Vc*DyP. Therefore, charged residues, such as histidine and aspartic acid, in the distal pocket do not present a key factor for the pH dependence of the dye degradation by *Vc*DyP.

Alterations in the radical transfer pathway through His178

Next, I focused on the radical transfer pathways. As described above, His178, which is located 4.3 Å apart from the edge of heme (Figure 2.8), is proposed as one of the residues that determine the radical transfer pathway from heme to the active site in *Vc*DyP.[7] In *Vc*DyP, radicals transferred to Tyr133 at higher pH are used to form cross-links with Tyr109 from a different subunit, but at lower pH, radicals are transferred to Tyr129 and/or Tyr235 to be used to decolorize dyes. To fix the radical transfer path to active site regardless of any pH, I introduced three aromatic residues (Phe, Trp, Tyr) at position 178.

In contrast to the H178L mutant[7], the H178F mutant was half as active as WT *Vc*DyP, indicating that an aromatic ring at this position aids in radical transfer from heme for dye decolorization. However, the pH profile of dye decolorization activity of the H178F mutant was similar to that of WT *Vc*DyP (Figure 2.5). Introduction of tryptophan or tyrosine at position 178 led to increasing the dye-degrading activity slightly at neutral pH (Figure 2.5). These results support the previous proposal that at pH 4.0, radicals generated at the heme of WT *Vc*DyP move to Tyr129/Tyr235 via His178 where dye substrates are decomposed, while at pH 7.0, radicals move to Tyr133 and are consumed to form an intersubunit covalent bond with Tyr109 (Figure 2.12).

Substitution of Asp138 that forms a hydrogen bond with His178 with valine rendered the protein almost inactive at pH 4.0, but more active that the WT enzyme at pH >6.5 (Figure 2.9). The 80% loss of activity upon incubation at 25°C for 100 s suggests that the low activity is due to low protein stability at acidic pH. However, the guaiacol oxidation activity of the mutant at pH 4.0 was significantly higher than that of WT enzyme (Figure 2.10). These results support the previous proposal that radical transfer from heme to active site is controlled by His178; at pH 4.0, radicals generated at the heme of WT *Vc*DyP move

to Tyr129/Tyr235 via His178 where dye substrates are decomposed, while at pH 7.0, radicals move to Tyr133 and are consumed to form an covalent bond with Tyr109[7].

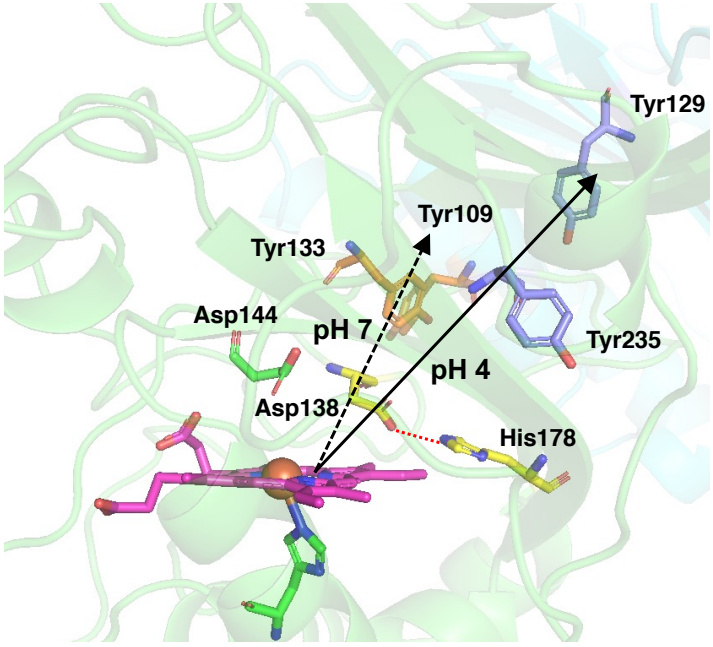

Figure 2.12 Putative pH-dependent radical transfer. At pH 7.0, radical transfer occurs from heme to Tyr109 or Tyr133 to form an intermolecular covalent bond between tyroshines. At pH 4, radical transfer occurs from heme to Tyr129 and Tyr235 to degrade dye substrate.

pH dependence of the dye-decolorizing activity of *Vc*DyP

The optimal pH for RB19 decolorization by WT *Vc*DyP is 4.5 (Figure 2.3). Michaelis-Menten analysis showed that K_m of WT enzyme at pH 4.5 (30 ± 3 μM) was only ~2-fold lower than that at pH 7.0 (66 ± 34 μM) (Table 2.2), indicating that substrate binding is not a factor underlying low activity at neutral pH. While the change in K_m does not account for the enhancement of *Vc*DyP activity at pH ~4, the extremely large k_{cat} may be a contributory factor. Under low pH conditions, the hydrogen bond between His178 and

Asp138 is cleaved by protonation of Asp138, causing conformational changes and facilitating radical transfer from heme to Tyr129/Tyr235 rather than Tyr109/Tyr133 (Figure 2.12). Minimal changes were observed for the Thr278 mutant (Figure 2.9), which also forms a hydrogen bond with His178 (Figure 2.6), suggesting that the hydrogen bond between Asp138 and His178 is necessary for dye decolorization by *Vc*DyP, but not that between His178 and Thr278. The optimal pH of the D138V mutant was shifted to pH 6.5. Since aspartic acid with pK_a of side-chain of ~4 is absent in the D138V mutant, the shift in optimal pH towards neutral pH may account for the pK_a of His178 (Figure 2.9). Accordingly, I propose that the pK_a of Asp138, but not Asp144, contributes to pH dependence of the dye-decolorizing activity of WT *Vc*DyP (Figure 2.9). Collectively, our data support a key decisive role of this hydrogen bond in the pH dependence of dye decolorization activity of DyPs.

Table 2.2: Kinetic constants (K_m, k_{cat}, and k_{cat}/K_m) of DyP for RB19.

		RB19		
		K_m	k_{cat}	k_{cat}/K_m
DyP	pH	μM	s^{-1}	s^{-1} μM^{-1}
WT	4.5	30 ± 3	2.3 ± 0.1	0.077 ± 0.011
WT	7.0	66 ± 34	0.014 ± 0.003	$(2.1 \pm 1.5) \times 10^{-4}$
D138V[28]	6.5	0.53 ± 0.23	0.47 ± 0.03	0.89 ± 0.45
D138V[28]	4.0	2.9 ± 1.0	0.17 ± 0.02	0.059 ± 0.026

Activation mechanism of D138V *Vc*DyP

Although I expected to increase k_{cat} for RB19 decolorization in D138V *Vc*DyP, no significant change was observed apart from increased K_m (Table 2.2)[28]. From the crystal structure of *Vc*DyP, there are four large pockets for substrate binding[7]. Pocket 1 is the heme distal pocket, a small substrate-binding site, such as H_2O_2 and guaiacol. Pocket 3 is potentially a large hydrophobic substrate-binding site, such as RB19, owing to its location at the subunit-subunit interface surrounded by Tyr129 and Tyr235 (Figure 2.13)[7]. However, Asp138 is located more than 10 Å from the edge of Pocket 3 and does not seem to affect its structure. Asp138 is located near Pocket 2. The absence of Tyr 129 and Tyr235 near Pocket 2 suggests that Pocket 2 is not a RB19 binding. The ~10-fold decrease in K_m for RB19 due to the mutation of Asp138 indicates that the structure of Pocket 2 is altered by the substitution, leading to a decrease in K_m. Considering that Asp138 is located near the edge of Pocket 2 and mutation of Asp138 results in a decrease in K_m, I propose that Asp138 controls dye-decolorizing activity through the structure of Pocket 2.

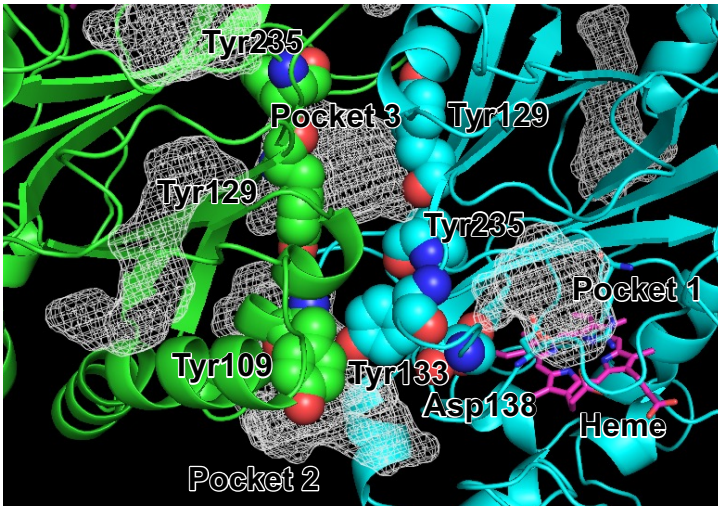

Figure 2.13 Ligand binding pocket of *Vc*DyP predicted using POCASA.[31,32]

Binding affinity of *Vc*DyP to heme in *E. coli*

I expected that *E. coli* expressing the D138V *Vc*DyP, which can degrade RB19 at neutral pH, could regrade the dye, but the activity was low. One possible cause of reduced activity could be that *Vc*DyP is mainly expressed in a heme-free form, which cannot react with H_2O_2. *Vc*DyP from *E. coli* requires the reconstruction with hemin in *viro*.[7,28] In the heterologous expression system using *E. coli, Vc*DyP does not bind heme and instead Protoporphyrin IX (PPIX), which was absence of heme iron (Figure 2.14). From previous studies, the value of the dissociation constant K_d of *Vc*DyP for heme was determined to be 72 ± 5 nM[7], which was 100-fold higher than that of myoglobin (0.59 nM)[29], which is expressed with heme in the cell, suggesting that the mutant *Vc*DyP cannot bind a sufficient amount of heme in *E. coli*. Therefore, I considered it necessary to create a persistent dye-degrading enzyme using a protein that is attached to heme in cells.

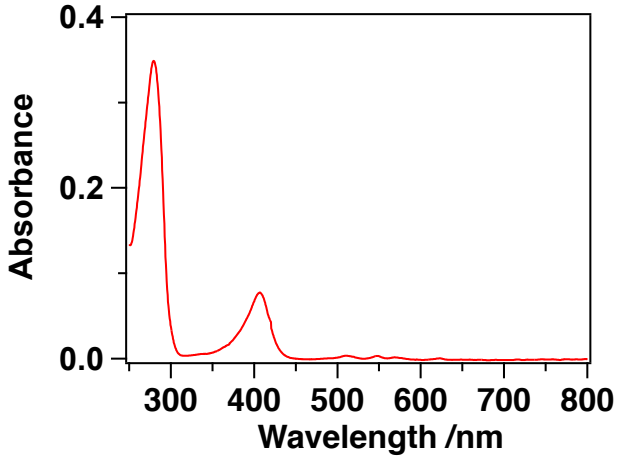

Figure 2.14 The absorbance of the purified *Vc*DyP. The small peaks at 500~600 nm are derived from protoporphyrin IX.

In summary, I found the key factor of the pH dependence of the dye-decolorizing activity of *Vc*DyP. Asp144 at the heme distal site is necessary for DyP activity but does not contribute to pH dependence. Mutation of Asp138 to valine shifted the optimal pH to 6.5, with concomitant ~10-fold higher catalytic efficiency relative to WT *Vc*DyP at pH 4.5. I propose that a hydrogen bond between His178 and Asp138 plays a key role in pH-dependent dye-decolorizing activity, through alterations in the radical transfer pathway. On the other hand, *E. coli* expressing D138V *Vc*DyP had low dye degradation activity. The problem is that heme is not coordinated to this enzyme. To solve this problem, in the next chapter I describe an artificial enzyme design using cytochrome *c*, which is attached to heme in cells.

References

1. Sugano, Y., Muramatsu, R., Ichiyanagi, A., Sato, T. & Shoda, M. DyP, a unique dye-decolorizing peroxidase, represents a novel heme peroxidase family: ASP171 replaces the distal histidine of classical peroxidases. J. Biol. Chem., **282**, 36652–36658 (2007).
2. Sugano, Y., Matsushima, Y., Tsuchiya, K., Aoki, H., Hirai, M. & Shoda, M. Degradation pathway of an anthraquinone dye catalyzed by a unique peroxidase DyP from Thanatephorus cucumeris Dec 1. Biodegradation, **20**, 433–440 (2009).
3. van Bloois, E., Torres Pazmiño, D. E., Winter, R. T. & Fraaije, M. W. A robust and extracellular heme-containing peroxidase from Thermobifida fusca as prototype of a bacterial peroxidase superfamily. Appl. Microbiol. Biotechnol., **86**, 1419–1430 (2010).
4. Sugano, Y., Muramatsu, R., Ichiyanagi, A., Sato, T. & Shoda, M. DyP, a unique dye-decolorizing peroxidase, represents a novel heme peroxidase family: ASP171 replaces the distal histidine of classical peroxidases. J. Biol. Chem., **282**, 36652–36658 (2007).
5. Lučić, M., Svistunenko, D., Wilson, M., Chaplin, A., Davy, B., Ebrahim, A., Axford, D., Tosha, T., Sugimoto, H., Owada, S., Dworkowski, F., Tews, I., Owen, R., Hough, M., & Worrall, J. Serial Femtosecond Zero Dose Crystallography Captures a Water-Free Distal Heme Site in a Dye-Decolorising Peroxidase to Reveal a Catalytic Role for an Arginine in FeIV=O Formation. Angew. Chem. Int., **59**, 21656–21662 (2020).
6. Lučić, M. Chaplin, A., Moreno-Chicano, T., Dworkowski, F., Wilson, M., Svistunenko, D., Hough, M., & Worrall, J. A subtle structural change in the distal haem pocket has a remarkable effect on tuning hydrogen peroxide reactivity in dye decolourising peroxidases from: Streptomyces lividans. Dalton Trans., **49**, 1620–1636 (2020).
7. Uchida, T., Sasaki, M., Tanaka, Y. & Ishimori, K. A Dye-Decolorizing Peroxidase from Vibrio cholerae. Biochemistry, **54**, 6610–6621 (2015).
8. Strittmatter, E., Liers, C., Ullrich, R., Wachter, S., Hofrichter, M., Plattner, D. & Piontek, K. First crystal structure of a fungal high-redox potential dye-decolorizing peroxidase substrate interaction sites and long-range electron transfer. J. Biol. Chem., **288**, 4095–4102 (2013).
9. Shrestha, R., Chen, X., Ramyar, K., Hayati, Z., Carlson, E., Bossmann, S., Song, L., Geisbrecht, B. & Li, P. Identification of surface-Exposed protein radicals and a substrate oxidation site in a-Class dye-Decolorizing peroxidase from

thermomonospora curvata. ACS Catal., **6**, 8036–8047 (2016).

10. Baratto, M., Sinicropi, A., Linde, D., Sáez-Jiménez, V., Sorace, L., Ruiz-Duenas, F., Martinez, A., Basosi, & R. Pogni, R. Redox-Active Sites in Auricularia auricula-judae Dye-Decolorizing Peroxidase and Several Directed Variants: A Multifrequency EPR Study. J. Phys. Chem. B., **119**, 13583–13592 (2015).
11. Chaplin, A. Chicano, T., Hampshire, B., Wilson, M., Hough, M., Svistunenko, D. & Worrall, J. An Aromatic Dyad Motif in Dye Decolourising Peroxidases Has Implications for Free Radical Formation and Catalysis. Chem. Eur. J., **25**, 6141–6153 (2019)
12. Linde, D. Pogni, R., Cañellas, M., Lucas, F., Guallar, V., Baratto, M., Sinicropi, A., Sáez-Jiménez, V., Coscolin, C., Romero, A., Medrano, F., Ruiz-Dueñ;as, F. & Martínez, A. Catalytic surface radical in dye-decolorizing peroxidase: A computational, spectroscopic and site-directed mutagenesis study. Biochem. J., **466**, 253–262 (2015).
13. Beers, R. & Sizer, I. A spectrophotometric method for measuring the breakdown of hydrogen peroxide by catalase. J. Biol. Chem., **195**, 133–140 (1952).
14. Santimone, M. Titration Study of Guaiarcol Oxidation by Horseradish Peroxidase. Can. J. Biochem., **53**, 649–657 (1975).
15. Prytkova, T., Kurnikov, I., & Beratan, D. Ab initio based calculations of electron-transfer rates in metalloproteins. J. Phys. Chem. B., **109**, 1618–1625 (2005).
16. Kurnikov, I. V. HARLEM Molecular Modeling Package. (2000).
17. Beratan, D., Onuchic, N., Winkler, R. & Gray, B. Electron-tunneling pathways in proteins. Science., **258**, 1740–1741 (1992).
18. Ozaki, S., Matsui, T. & Watanabe, Y. Conversion of Myoglobin into a Highly Stereo- specific Peroxygenase by the L29H/H64L Mutation. J. Am. Chem. Soc., **118**, 9784–9785 (1996).
19. Matsui, T., Ozaki, S., Liong, E., Phillips, G. N. & Watanabe, Y. Effects of the Location of Distal Histidine in the Reaction of Myoglobin with Hydrogen Peroxide. J. Biol. Chem., **274**, 2838–2844 (1999).
20. Phillips, S. E. v. Structure and Refinement of Oxymyoglobin at l-6 A Resolution. J. Mol. Biol., **142,** 531-554 (1980).
21. Ozaki, S. I., Roach, M. P., Matsui, T. & Watanabe, Y. Investigations of the roles of the distal heme environment and the proximal heme iron ligand in peroxide activation by heme enzymes via molecular engineering of myoglobin. Acc. Chem, Res., **34**, 818–825 (2001).
22. Mendes, S., Brissos, V., Gabriel, A., Catarino, T., Turner, D., Todorovic, S., &

Martins, L. An integrated view of redox and catalytic properties of B-type PpDyP from Pseudomonas putida MET94 and its distal variants. Arch. Biochem. Biophys., **574**, 99–107 (2015).

23. Dunford, H. B. Heme peroxidases. John Wiley, New York. (1999).
24. Pfanzagl, V., Nys, K., Bellei, M., Michlits, H., Mlynek, G., Battistuzzi, G., Djinovic-Carugo, K., Van Doorslaer, S., Furtmüller, P., Hofbauer, S., & Obinger, C. Roles of distal aspartate and arginine of B-class dye-decolorizing peroxidase in heterolytic hydrogen peroxide cleavage. J. Biol. Chem., **293**, 14823–14838 (2018).
25. Chaplin, A. K., Wilson, M. T. & Worrall, J. A. R. Kinetic characterisation of a dye decolourising peroxidase from Streptomyces lividans: New insight into the mechanism of anthraquinone dye decolourisation. Dalton Trans., **46**, 9420–9429 (2017).
26. Brissos, V., Tavares, D., Sousa, A. C., Robalo, M. P. & Martins, L. O. Engineering a Bacterial DyP-Type Peroxidase for Enhanced Oxidation of Lignin-Related Phenolics at Alkaline pH. ACS Catal., **7**, 3454–3465 (2017).
27. Savenkova, M. I., Newmyer, S. L. & Ortiz de Montellano, P. R. Rescue of His-42 → Ala horseradish peroxidase by a Phe-41 → His mutation. Engineering of a surrogate catalytic histidine. J. Biol. Chem., **271**, 24598–24603 (1996).
28. Uchida, T., Omura, I., Umetsu, S. & Ishimori, K. Radical transfer but not heme distal residues is essential for pH dependence of dye-decolorizing activity of peroxidase from Vibrio cholerae. J. Inorg. Biochem., **219**, 111422 (2021).
29. Gryczynski, Z., Lubkowski, J. & Bucci, E. Heme-Protein Interactions in Horse Heart Myoglobin at Neutral pH and Exposed to Acid Investigated by Time-resolved Fluorescence in the Pico- to Nanosecond Time Range. J. Biol. Chem., **270**, 19232–19237 (1995).
30. W.L. DeLano. The PyMOL Molecular Graphics System. (2002).
31. Yu, J., Zhou, Y., Tanaka, I. & Yao, M. Roll: A new algorithm for the detection of protein pockets and cavities with a rolling probe sphere. Bioinformatics., **26**, 46–52 (2009).
32. Yan, C. & Zou, X. Predicting peptide binding sites on protein surfaces by clustering chemical interactions. J. Comput. Chem., **36**, 49–61 (2014).

CHAPTER III

Converting cytochrome *c* into a DyP-like metalloenzyme

Abstract

In this chapter, I present to design an artificial enzyme with high dye-degrading activity based on cytochrome *c* (cyt *c*), an electron transfer protein. I found that cyt *c* can degrade RB19, but the ability at pH 7.0 was ~60% of that of *Vc*DyP at pH 4.5. To enhance the activity, I constructed several mutants using three approaches. Initially, to improve the reactivity with H_2O_2, Met80 was replaced with a non-coordinating residue, Ala or Val, but catalytic efficiency (k_{cat}/K_m) was increased by only ~1.5-fold. Then, to enhance the substrate binding affinity, I introduced additional Trp at position 76. The catalytic efficiency of the mutant was ~3-fold larger than that of WT cyt *c*. Finally, to form a hydrogen bond to axial histidine, Gly29 was replaced with Asp (G29D). The mutant exhibited an ~80-fold larger dye-decolorizing activity. Although *E. coli* expressing the G29D mutant could not degrade the dye because the heme of this enzyme is readily degraded intracellularly, these results suggest that cyt *c* can be converted into a DyP-like enzyme based on rational design.

3.1 Introduction

In chapter II, I analyzed the reaction mechanism of *Vc*DyP, and succeeded in constructing the mutant which can degrade the persistent dye at neutral conditions. However, the mutant *Vc*DyP was not suitable for biocatalysts using *E. coli* because most DyP was expressed in a heme-free form.

In contrast to DyPs, the heme of cytochrome *c* (cyt *c*), which is a heme protein associated with electron transfer in the respiratory chain, is bound to the polypeptide through covalent bonds. whereas it can also work as peroxidase when Met80, one of the heme ligands, dissociates from the heme iron[1,2]. Several studies reported that dissociation of Met80 from heme is caused by the interaction of cyt *c* with cardiolipins in the mitochondrial membrane, leading to a significant increase (>50-fold) in the peroxidase activity[1]. This increase is accounted by the formation of pentacoordinate heme or hexacoordinated heme with a water bound, which increases the accessibility of H_2O_2 to the heme iron.

From these data, I conceived the idea that the degradation of anthraquinone dye using *E. coli* could be achieved by converting cyt *c* into an enzyme that efficiently degrades the dye under neutral pH and constructing an *E. coli* expressing this enzyme. In this chapter, I tried to design an artificial cyt *c* which could degrade persistent dye effectively using several approaches based on the structure of DyP and the dye-degradation reaction mechanism of DyP. I constructed the mutants according to each approach and analyzed dye-degradation activities and investigated the dye-degrading activity of *E. coli* expressing the mutant cyt *c*.

3.2 Experimental Procedures

Materials

All chemicals were purchased from Wako Pure Chemical Industries (Osaka, Japan), Nacalai Tesque (Kyoto, Japan), Kanto Chemical (Tokyo, Japan) or Sigma-Aldrich (St. Louis, USA) and used without further purification.

Protein expression and preparation

The *Escherichia coli* strain Rosetta 2(DE3)pLysS cells were transformed with the plasmids containing horse heart cyt *c* and yeast cyt *c* heme lyase[3,4]. They were inoculated in 5 mL of Luria-Bertani (LB) medium and grown overnight. This pre-cultured medium was added to 2 L of 2×TY medium supplemented with 100 μg L^{-1} ampicillin and 34 μg L^{-1} chloramphenicol, and the bacteria were further incubated at 37 °C. The expression of cyt *c* was initiated by adding 1 mM isopropyl β-D-thiogalactopyranoside (IPTG) to the culture when the cell density reached an optical density at 600 nm (OD_{600}) of 0.6. Then, 0.1 mM δ-aminolaevulinic acid was added to promote heme biosynthesis. After incubation at 25 °C for additional 24 h, the cells were collected by centrifugation.

The cell pellet was resuspended in 50 mM Tris-HCl, pH 7.5, containing 1 mg m L^{-1} lysozyme, 50 mg L^{-1} DNase I and RNase A, and suspended for 1 h to lysis the cell pellets completely. The supernatant of the crude extract was obtained by centrifugation at 18,000 rpm for 5 min. Ammonium sulfate was added to the supernatant to a concentration of 351 g L^{-1} while stirring at 4 °C. Following centrifugation, the supernatant was dialyzed (Spectra/Por, 6,000–8,000 M_r cutoff) overnight in 4 L of buffer A (50 mM sodium phosphate, pH 7.4) to remove ammonium sulfate. The sample was loaded onto a HiTrap SP HP column (Cytiva) with a linear gradient of 1–300 mM NaCl. The elusion sample

was concentrated by Amicon ultrafiltration using 3-kDa cutoff membranes. Because purified cyt *c* was a mixture of ferric and ferrous forms, it was oxidized by potassium ferricyanide and further purified by a gel-filtration column (HiLoad 16/60 Superdex 200 pg, Cytiva) equilibrated with 50 mM Tris-HCl and 150 mM NaCl (pH 8.0).

Site-directed mutagenesis

Mutagenesis was conducted utilizing the PrimeSTAR mutagenesis basal kit from Takara Bio (Otsu, Japan) using WT expression vector as the template. DNA oligonucleotides were purchased from Eurofins Genomics (Tokyo, Japan). Primers used for construction of mutants are listed in Table 3.1. Genes were sequenced (Eurofins Genomics) to ensure that only the desired mutations were introduced.

Table 3.1: Oligonucleotides used for construction of expression vectors for mutants. The underlined bases signify the introduced mutations.

Mutants	Primers (top, sense; bottom, anti-sense)
M80V	5′— ACGAAAGTGATCTTCGCGGGCATCAAA — 3′
	5′— GAAGATCACTTTCGTGCCCGGGATGTA — 3′
Y48H	5′— TTCACGCATACGGACGCGAACAAAAAC — 3′
	5′— GTCCGTATGCGTGAAGCCCGGCGCCTG — 3′
Y67H	5′— ATGGAACATCTCGAGAACCCGAAAAAA — 3′
	5′— CTCGAGATGTTCCATCAGCGTTTCTTC — 3′
Y74H	5′— AAAAAACATATCCCGGGCACGAAAATG — 3′
	5′— CGGGATATGTTTTTTCGGGTTCTCGAG — 3′
Y97H	5′— ATCGCGCATCTGAAAAAGGCGACGAAC — 3′
	5′— CGCGAAGACCTGATCGCGCATCTGAAA — 3′
P76W	5′— TACATCTGGGGCACGAAAATGATCTTC — 3′
	5′— CGTGCCCCAGATGTATTTTTTCGGGTT — 3′
G29D	5′— AAAACCGACCCCAACCTGCACGGCCTG — 3′
	5′— GTTGGGGTCGGTTTTGTGTTTGCCGCC — 3′

Dye-decolorizing assay

Dye-decolorizing activity was determined by spectrophotometrically measuring the rate of H_2O_2-mediated decomposition of RB19. Briefly, 1.9 mL of protein solution (final concentration of 1 μM) in 50 mM sodium phosphate (pH 7.0) was placed in a 2 mL cuvette, along with 10–50 μL of the substrate solution to be tested. The reaction was started by the addition of 3.3 μL of 12 M H_2O_2 (final concentration of 20 mM) in the same buffer, with incubations normally for 5 min at room temperature. The decomposition of the substrate was measured at 595 nm (ε_{595} = 10 mM^{-1} cm^{-1}) using a JASCO V-550 spectrophotometer. H_2O_2 concentrations were determined spectrophotometrically using an absorption coefficient at 240 nm of 43.6 M^{-1} cm^{-1}.[5] The curve of initial rates (v) *versus* H_2O_2 concentrations was fitted to the Michaelis-Menten equation:

$$v/[\text{protein}] = k_{cat}[H_2O_2]/(K_m + [H_2O_2]) \quad (1)$$

where k_{cat} and K_m are maximum rate and Michaelis-Menten constant, respectively. The curve of initial rates versus RB19 concentrations were fitted better to the Hill equation:

$$v/[\text{protein}] = k_{cat}[\text{RB19}]^h/[(K_d)^h + [\text{RB19}]^h] \quad (2)$$

where h and K_d are the Hill constant and apparent dissociation constant, respectively.

The turnover rate of the dye-decolorizing activity was calculated by measuring the decrease in absorbance at 595 nm 100 s after initiating the reaction and reported in min^{-1}.

Peroxidase assay

The peroxidase assay was measured spectrophotometrically. The standard assay was performed in 2 mL of the reaction mixture with the enzyme, 10 mM H_2O_2, and an appropriate amount of guaiacol (5−150 μM) at 25 °C. The concentrations of the proteins were 0.1 μM (M80A, M80V, G29D) or 1 μM (WT and P76W) for guaiacol. The reaction was initiated with the addition of H_2O_2, and the initial rate for guaiacol oxidation was monitored at 470 nm (ε_{470} = 22.6 mM^{-1} cm^{-1}). Data were fitted to the Michaelis–Menten equation. Rapid reaction of cyt *c* with H_2O_2 were monitored with a stopped-flow apparatus (MSP-1000-V; Unisoku, Osaka, Japan).

Dye-decolorizing assay using *E. coli* overexpressed mutant enzymes

E. coli BL21(DE3) transformed with the pET26b(+) cyt *c* vector and pEC86 vector was incubated in Luria-Bertani (LB) media at 37 ºC under shaking at 200 rpm. 1 mM of isopropyl-β-D-1-thiogalactopyranoside (IPTG), 0.1 mM δ-aminolaevulinic acid, and 40 μM RB19 were added when the optical density at 600 nm (OD_{600}) reached 0.6.

After 24 hours of incubation, the supernatant of the culture medium was collected by centrifugation, and the change in absorbance of RB19 in the supernatant was measured using a V-570 spectrophotometer (Jasco, Tokyo, Japan).

3.3 Results

3.3.1 Dye-decolorizing activity of cyt *c*

I first measured the dye-decolorizing activity of cyt *c* at pH 7.0 using RB19 as a substrate. The activity was monitored using UV-visible absorption spectroscopy. The characteristic absorbance of RB19 around 595 nm decreased after manually mixing of cyt *c* with H_2O_2 (20 mM) (Figure 3.1A), and the blue solution turned colorless within 300 s. The result indicated that cyt *c* has a dye-decolorizing activity. To determine steady-state kinetic parameters (maximum rate, k_{cat} and Michaelis-Menten constant, K_m), the reactions were performed at a fixed concentration of RB19 (200 μM) at pH 7.0. The initial rates of RB19 degradation were obtained by fitting the decay of the absorption at 595 nm. The data were fitted to the Michaelis-Menten equation (equation 1) (Figure 3.1B), which provided $k_{cat,H2O2}$ of 5.6 ± 0.4 s^{-1} and $K_{m,H2O2}$ of 30 ± 4 mM.

I next monitored kinetic of the dye-decolorizing activity of cyt *c*, and the decolorizing assay was carried out at a fixed concentration of H_2O_2 (20 mM). The initial rates were plotted against the concentrations of RB19 (Figure 3.1C). Kinetic data were fitted better to the Hill equation, (equation 2) rather than the Michaelis-Menten equation. The evaluated $k_{cat,RB19}$ and $K_{m,RB19}$ values were of 2.3 ± 0.1 s^{-1} and 53 ± 6 μM, respectively. The $k_{cat,RB19}$ value of cyt *c* was close to that of *Vc*DyP at the optimal pH, whereas the $K_{m,RB19}$ of cyt *c* was slightly larger than that of *Vc*DyP (Table 3.2). Therefore, the $k_{cat,RB19}/K_{m,RB19}$ of cyt *c* was 57% of that of *Vc*DyP.

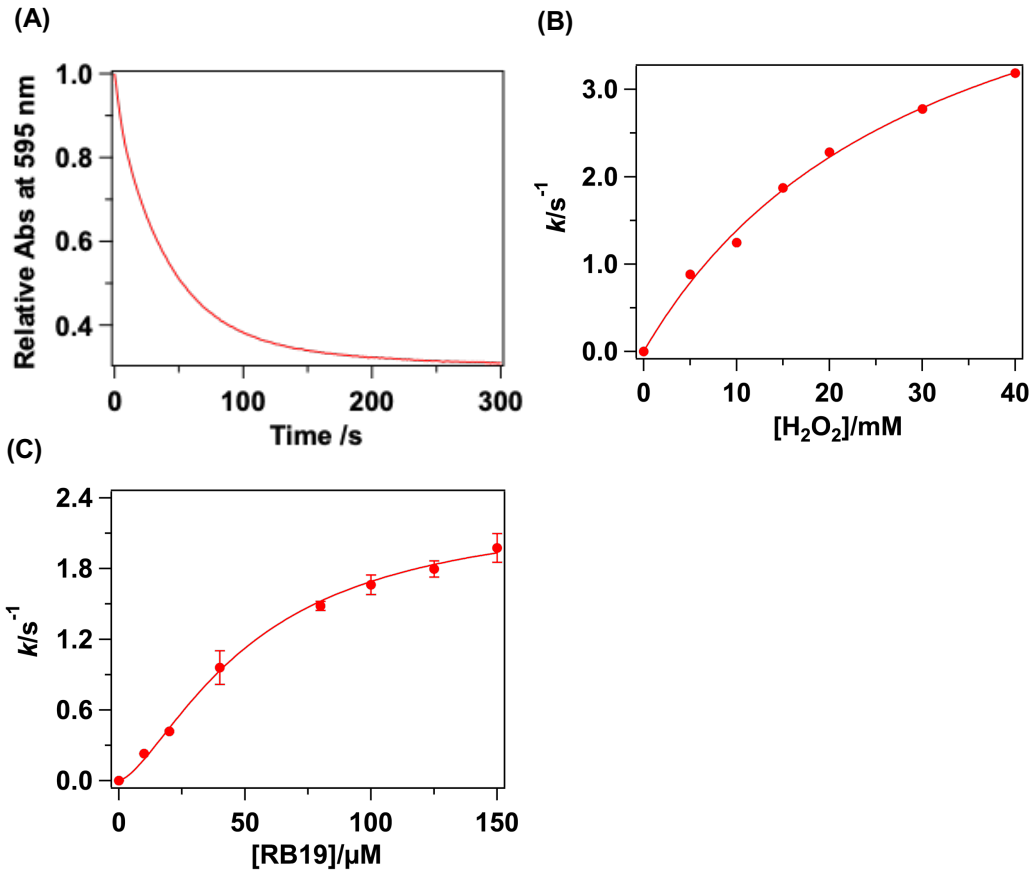

Figure 3.1 Dye-decolorizing activity of WT cyt *c*. (A) Time-course of the dye-decolorizing reaction by WT cyt *c* at pH 7.0. The kinetic change of absorption at 595 nm during the reaction of cyt *c* (1.0 μM) and RB19 (40 μM) with H_2O_2 (20 mM) at 25 °C. (B) Initial rate ($k = v$/[protein] in eqn (1)) of RB19 (200 μM) oxidation at various concentrations (protein, 1.0 μM; pH 7.0). (C) Steady-state rates of oxidation as a function of RB19 concentration (0–150 μM) catalyzed by WT cyt *c* at pH 7.0.

3.3.2 Replacing the sixth axial ligand with a non-coordinating amino acid residue

I confirmed dye-decolorizing activity of cyt *c*, which was comparable (~60 %) to that of *Vc*DyP at pH 4.5 (Table 3.2). However, this assay was conducted at relatively high concentration of H_2O_2 (20 mM). The turnover of the dye-decolorizing assay of cyt *c* was calculated to be 0.7 min^{-1} at low H_2O_2 concentration (200 μM H_2O_2), which was only ~2% of that of *Vc*DyP (36 min^{-1}). Thus, the dye-degrading activity of cyt *c* needs higher concentrations of H_2O_2 than *Vc*DyP. Previous studies have shown that replacing the sixth axial ligand (Met80) of cyt *c* with Val increases the accessibility of H_2O_2 to heme, leading to enhancement (~10-fold) of the peroxidase activity[6,7]. Accordingly, I expected that replacing Met80 with non-coordinating amino acids, Ala (M80A) or Val (M80V) increases the dye-decolorizing activity. The activity of the variants was evaluated by examining the initial rates of RB19 oxidation (Figure 3.2A). Kinetic data showed that the $k_{cat,RB19}$ of dye-decolorizing activities of the M80A and M80V mutants were 2.4 ± 0.3 s^{-1} and 3.4 ± 0.1 s^{-1}, respectively. The $K_{m,RB19}$ of these mutants were 54 ± 13 μM, 49 ± 3 μM, respectively (Table 2). The k_{cat} of the M80V mutant was slightly larger than that of WT (2.3 ± 0.1 s^{-1}) and the K_m was similar to that of WT (53 ± 6 μM), leading to ~1.5-fold increase in the catalytic efficiency ($k_{cat,RB19}/K_{m,RB19}$). Although I expected that the substitution of Met80 would significantly improve the dye-degradation activity of cyt *c*, it did not happen.

In order to confirm whether the reactivity of heme with H_2O_2 was enhanced by the mutation of Met80 as expected, the steady-state kinetics of the M80A and M80V mutants were studied using a typical peroxidase substrate, guaiacol (Figure 3.2B). The kinetic data at pH 7.0 showed that the $k_{cat,guaiacol}$ of peroxidase activities of the M80A and M80V mutants were 1.22 ± 0.04 and 2.6 ± 0.1 s^{-1}, respectively, which were 13 and 27-fold larger

than that of WT cyt *c*, respectively. The $K_{m,guaiacol}$ of the M80A and M80V mutants were 5.6 ± 0.9 and 2.9 ± 0.4 μM, which were almost the same as and half of that of WT cyt *c*, respectively. The $k_{cat,guaiacol}/K_{m,guaiacol}$ values of the two variants were ~14–56-fold larger than that of WT cyt *c*. The value of the M80A and M80V mutant were ~3 and ~12-fold larger than that of native HRP [8] (Table 3.3), indicating that both mutants are good peroxidase. Considering that the peroxidase activities ($k_{cat,guaiacol}/K_{m,guaiacol}$) of the mutants were ~13–56-fold larger than that of WT cyt *c*, whereas the dye-degrading activities ($k_{cat,RB19}/K_{m,RB19}$) of them were less than 2-fold larger than that of WT cyt *c*. Therefore, elimination of Met80 was effective in enhancing the peroxidase activity, but it did not contribute to the enhancement of the dye-degradation activity. The comparable $K_{m,RB19}$ value of the Met80 mutants to WT cyt *c* suggests that the radicals formed at heme by the reaction with H_2O_2 are not efficiently transferred to the active site or radicals transferred to the active site are not utilized well for dye degradation.

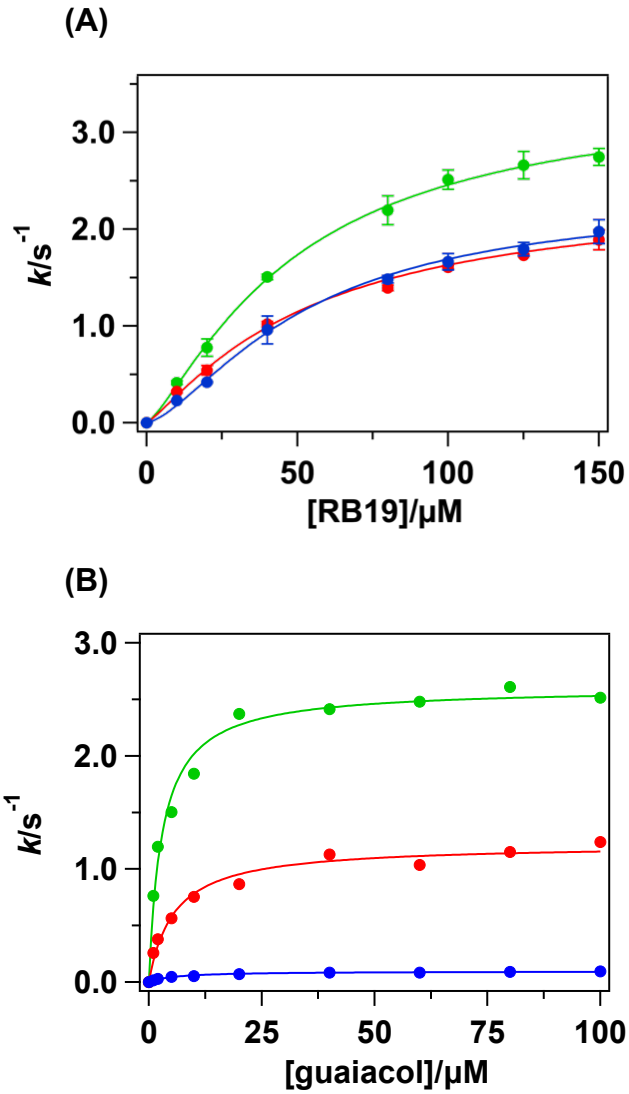

Figure 3.2 Kinetic analysis of the H_2O_2-dependent reaction of WT (blue), M80A (red), and M80V (green). (A) Initial rates ($k = v$/[protein]) of oxidation as a function of RB19 concentration (0–150 μM) by proteins (protein, 1.0 μM; H_2O_2, 20 mM; pH 7.0). (B) Initial rates of oxidation as a function of guaiacol concentration (0–100 μM) catalyzed by proteins at pH 7.0 (WT, 1.0 μM; M80A and M80V, 0.1 μM; H_2O_2, 10 mM; pH 7.0).

Table 3.2 Kinetic parameters of WT cyt *c* and its mutants for RB19 decolorization

Proteins	RB19		
	k_{cat} (s^{-1})	K_m (μM)	k_{cat}/K_m (s^{-1} mM^{-1})
WT	2.3 ± 0.1	53 ± 6	44 ± 6
M80A	2.4 ± 0.3	54 ± 13	45 ± 12
M80V	3.4 ± 0.1	49 ± 3	70 ± 5
P76W	3.4 ± 0.1	25 ± 2.0	138 ± 12
G29D	2.5 ± 0.1	0.70 ± 0.10	3625 ± 483
Y48H/M80A	1.5 ± 0.1	19 ± 4	77 ± 17
Y67H/M80A	2.6 ± 0.1	60 ± 3	44 ± 3
Y74H/M80A	2.5 ± 0.1	31 ± 3	80 ± 8
Y97H/M80A	1.8 ± 0.1	52 ± 6	34 ± 4
*Vc*DyP	2.3 ± 0.1	30 ± 3	77 ± 11
F43Y/F138W/P88W Mb[9)]	9.6 ± 0.2	8 ± 1	1200

Table 3.3 Kinetic parameters of WT cyt *c* and its mutants for guaiacol oxidation

Proteins	guaiacol		
	k_{cat} (s^{-1})	K_m (μM)	k_{cat}/K_m (s^{-1} mM^{-1})
WT	0.096 ± 0.003	5.9 ± 0.8	16 ± 2
M80A	1.22 ± 0.04	5.6 ± 0.9	218 ± 36
M80V	2.6 ± 0.1	2.9 ± 0.4	896 ± 13
P76W	0.085 ± 0.001	8.3 ± 0.5	10 ± 1
G29D	1.57 ± 0.03	0.9 ± 0.1	1777 ± 203
native HRP[6)]	420 ± 40	5800 ± 700	72

3.3.3 Replacement of surface tyrosine with histidine

According to the previous studies, the active site of dye-decolorizing reaction of DyPs is Tyr or Trp at the protein surface[10–13], to which radicals formed at heme transfer. In the case of *Vc*DyP, Tyr129 and Tyr235 are the putative active site of the dye-decolorizing reaction[10]. Cyt *c* has four Tyr (Tyr48, Tyr67, Tyr74, and Tyr97), all of which are located on the protein surface (Figure 3.3) and has also one Trp (Trp59) that is buried inside the protein. Therefore, I supposed that radicals generated by the reaction of heme with H_2O_2 is transferred to one or some of these four tyrosine residues. To determine the active site of dye-degradation by cyt *c*, I prepared four Tyr mutants (Y48H/M80A, Y67H/M80A, Y74H/M80A, and Y97H/M80A), in which each Tyr and Met80 were replaced with His and Ala, respectively, and their dye-decolorizing activity was evaluated.

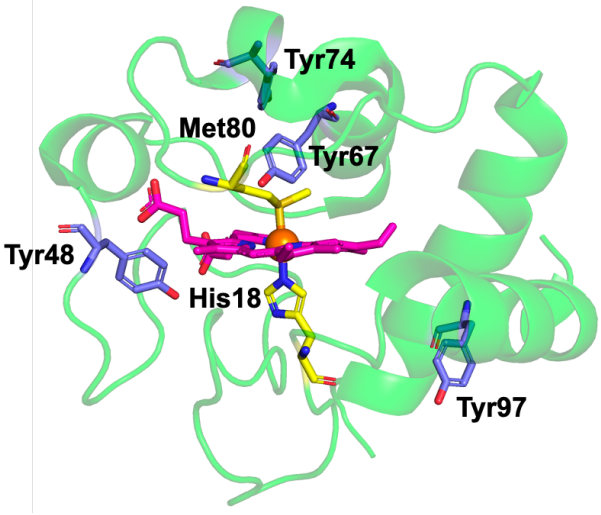

Figure 3.3 Location of Tyr48, Tyr67, Tyr74, Tyr97 in cyt *c* (PDB 6K9I).

Kinetic data analysis provided the $k_{cat,RB19}$ of the dye-decolorizing activities of 1.5 ± 0.1 (Y48H/M80A), 2.6 ± 0.1 (Y67H/M80A), 2.5 ± 0.1 (Y74H/M80A) and 1.8 ± 0.1 s^{-1} (Y97H/M80A) (Table 3.2). The $K_{m,RB19}$ of these mutants were 19 ± 4 (Y48H/M80A), 60 ± 3 (Y67H/M80A), 31 ± 3 (Y74H/M80A), and 52 ± 6 μM (Y97H/M80A) (Table 3.2).

The $k_{cat,RB19}$ of these mutants are not much larger than that of WT cyt *c*, whereas the $K_{m,RB19}$ of the Y48H/M80A and Y74H/M80A mutants were ~1/3 and ~1/2 of that of WT, respectively. A more prominent feature of the Y48H/M80A and Y74H/M80A mutants is the presence of a lag-phase at < 20 mM of H_2O_2 (Figure 3.4). In the kinetic characterization of DyP from *Streptomyces lividans*, the presence of a lag-phase at low RB19 concentration is considered that the rate-limiting step of the dye-decolorizing reaction is the disproportionation between dye radical[14]. The Hill plots for Y48H/M80A and Y74H/M80A mutants suggested that the affinity of cyt *c* for the substrate at low concentrations of RB19 was weakened by replacement of Tyr48 or Tyr74 with His and the disproportionation rate of the dye in the solution would be decelerated. Therefore, Tyr48 and Tyr74 are the putative active sites of the dye-degradation reaction.

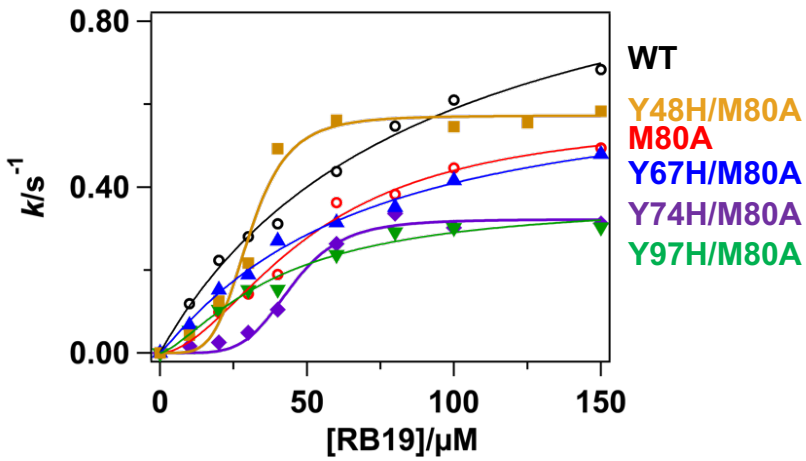

Figure 3.4 Kinetic analysis of the H_2O_2-dependent reaction of WT (black), M80A (red), Y48H/M80A (ocher), Y67H/M80A (blue), Y74H/M80A (purple) and Y97H/M80A (green). Initial rates ($k = v$/[protein]) of oxidation as a function of RB19 concentration (0–150 μM) with H_2O_2 (10 mM) catalyzed by proteins at pH 7.0.

3.3.4 Dye-decolorizing activity of P76W cyt *c* derivatives

Since Tyr48 and/or Tyr74 were suggested to be the active sites, we attempted to increase the affinity of the substrate by introducing a hydrophobic residue near these residues. From the crystal structure of cyt *c*[15], Pro76 is located between Tyr48 and Tyr74, and its side chain is exposed to the solvent (Figure 3.5). Therefore, I constructed a mutant, in which Pro76 was replaced with Trp (P76W) and measured dye-decolorizing activity. The obtained rate constants were plotted against the substrate concentration and fit to the Hill-equation (Figure 3.6). The $k_{cat,RB19}$ was 3.4 ± 0.1 s^{-1}, which was slightly higher than that of WT (2.3 s^{-1}), whereas the $K_{m,RB19}$ of the P76W mutant cyt *c* was 25 ± 2 μM, almost half of that of WT (53 μM) (Table 3.2). As a result, the $k_{cat,RB19}/K_{m,RB19}$ value of the P76W mutant was 138 s^{-1} mM^{-1}, ~3-fold larger than that of WT cyt *c* (44 s^{-1} mM^{-1}) (Table 3.2).

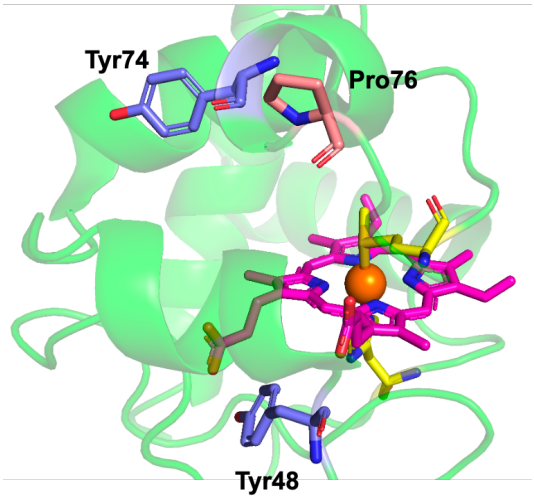

Figure 3.5 Location of Tyr48, Tyr74, and Pro76, in cyt *c*.

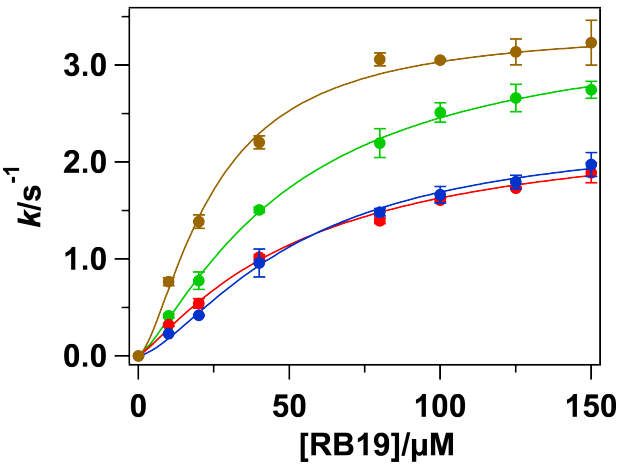

Figure 3.6 Kinetic analysis of the H_2O_2-dependent reaction of WT (blue), M80A (red), M80V (blue), and P76W (ocher). Kinetic of oxidation as a function of RB19 concentration (0-150 μM) with H_2O_2 (20 mM) catalyzed by proteins at pH 7.0.

3.3.5 Introduction of the proximal hydrogen bond

In most heme peroxidases, the proximal His forms a hydrogen bond with nearby Asp or Glu[16]. The hydrogen bond imparts more imidazolate character to the His ligand, increasing its electron donating ability and facilitating formation of compound I intermediate. In order to promote the generation of radicals to improve the dye degradation activity, I intended to introduce the proximal hydrogen bond into cyt *c*. On the basis of the crystal structure of cyt *c* (PDB code: 6K9I), Gly29 is located ~4 Å from proximal His (the distance between C_α of Gly29 and N_δ of His18 is 4.0 Å), and I constructed a mutant of Gly29 to Asp (G29D), which is presumed to be within hydrogen bond distance to the proximal His (Figure 3.7).

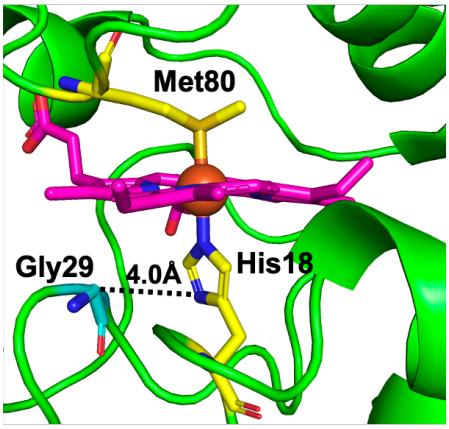

Figure 3.7 Location of His18 and Gly29 in cyt *c*. The distance between His18 and Gly29 are presented in the dotted line.

To provide insights into the dye-decolorizing activity of the G29D mutant, I measured the dye-decolorizing activity of the mutant (Figure 3.8A). As shown in Table 3.2, the G29D mutant exhibited almost the same $k_{cat,RB19}$ value and dramatically decreased $K_{m,RB19}$ compared to those of WT cyt *c*, resulting in ~80-fold higher overall catalytic efficiency ($k_{cat,RB19}/K_{m,RB19}$). The peroxidase activity of the mutant was also monitored using guaiacol under the steady state conditions. The obtained rate constants were plotted against the substrate concentrations and the plots were fit to the Michaelis–Menten equation (Figure 3.8B), $k_{cat,guaiacol}$ and $K_{m,guaiacol}$ were 1.57 ± 0.03 s^{-1} and 0.9 ± 0.1 μM, respectively (Table 3.3). As a result, the mutant exhibited a significant large catalytic efficiency ($k_{cat,guaiacol}/K_{m,guaiacol}$) of 1777 ± 203 s^{-1} mM^{-1}, which was ~110-fold larger than that of WT cyt *c*.

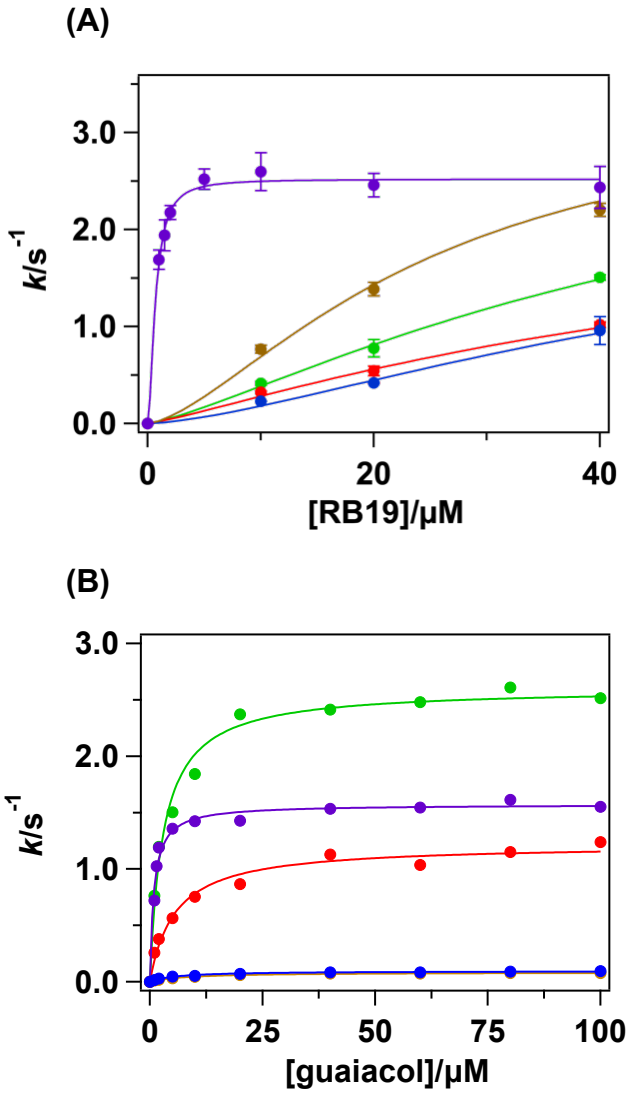

Figure 3.8 Kinetic analysis of the H_2O_2-dependent reaction of WT (blue), M80A (red), M80V (blue), and P76W (ocher), and G29D (purple). (A) Steady-state rates of oxidation as a function of RB19 concentration (0-40 μM) catalyzed by proteins at pH 7.0. (B) Steady-state rates of oxidation as a function of guaiacol concentration (0-100 μM) catalyzed by proteins at pH 7.0.

3.3.6 Whole-cell biocatalyst using the G29D mutant cyt *c*

Finally, the G29D mutant was used as a whole-cell catalyst. The mutant was expressed in the periplasmic space, where substrates are more easily accessible than in the cytoplasm. Coexpression with cytochrome *c* maturation proteins (pEC86) helps cyt *c* form covalent bonds (thioether bonds) with heme. The decolorizing abilities of *E. coli* were monitored as the decrease in absorbance at 595 nm over time (Figure 3.9A and B). The absorption spectrum of the culture medium containing RB19 changed little after 24 hours and thus *E. coli* expressing the G29D mutant did not degrade RB19 in the medium.

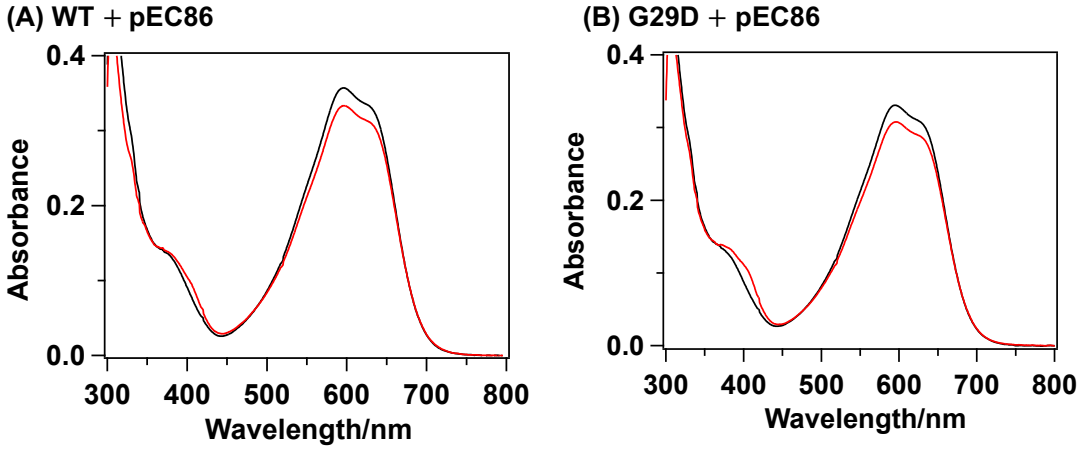

Figure 3.9 Absorbance of the supernatant of culture medium with RB19 (40 μM) of *E. coli* expressed (A) WT cyt *c* + pEC86, (B) G29D cyt *c* + pEC86 ;0h (black line) and 24h (red line).

3.4 Discussion

Introduction of additional Trp near the putative RB19 binding site

As described above, the $K_{m,RB19}$ of the P76W mutant was reduced by half of that of WT cyt *c*, as expected (Table 3.2). In the study of myoglobin mutants, the F43Y/F138W mutant with an additional introduction of Trp88 to the protein surface resulted in a ~10-fold smaller $K_{m,RB19}$ than that of WT Mb[9]. The results of docking simulations of this mutant with RB19 showed that the indole ring of Trp88 and the anthracene ring of RB19 adopted almost parallel structures, which indicates a π-π stacking interaction[9]. The kinetics data of the P76W mutant cyt *c* suggested that the substrate affinity of the mutant was increased by the hydrophobic interaction between RB19 and Trp76, but not as pronounced as the F43Y/F138W/Trp88 mutant.

Cyt *c* contains three Ω-loop regions, namely distal (residues 71–85), central (residues 40–57), and proximal (residues 12–28 and 29–39) Ω-loop[15,17]. The flexibility of the loops affects the heme pocket structure[18]. Pro76 is located in the 71-85 Ω-loop. Previous studies reported that an yeast iso-1-cyt *c* mutant, whose Phe82 was replaced with Gly, had a 10-fold higher ability to oxidize polycyclic aromatic hydrocarbons than WT yeast iso-1-cyt *c*[19], and increased the azide binding rate by ~6-fold[20]. Recent studies on human cyt *c* showed that $k_{cat,guaiacol}$ of the mutant of Ile81 in the loop with Ala (I81A) was ~10-fold larger than that of WT cyt *c*[21] , and $k_{cat,ABTS}$ of Pro76 with Cys (P76C) was 13-fold larger than that of WT cyt *c*[22]. These data are interpreted that mutation of amino acid residues in the 71-85 Ω-loop destabilizes coordination of Met80, which contributes to the increased peroxidase activity. However, the $k_{cat,guaiacol}/K_{m,guaiacol}$ value of the P76W mutant was 10 s^{-1} mM^{-1}, which was 60% that of WT (Table 3.3). As a result, introduction of Trp

near the putative active site for RB19 did not contribute to improvement of the catalytic efficiency as expected.

Effect of introduction of Asp near the heme on the structure of cyt *c*

In order to introduce this proximal hydrogen bond in cyt *c*, I constructed the G29D mutant. The absorption spectrum of the supernatant of the lysate of *E. coli* expressing WT cyt c has a split Q-band, characteristic of ferrous heme, whereas that of the G29D mutant did not, indicating conversion to the ferric form (Figure 3.10 A). Although the formation of the proximal hydrogen bond was not clear, the data suggest that the purified G29D mutant was easily oxidized, indicating the change in the redox potential of heme. The G29D mutant, which mimic the structural feature of heme peroxidases, dramatically enhanced $k_{cat,RB19}/K_{m,RB19}$ (Table 3.2) and $k_{cat,guaiacol}/K_{m,guaiacol}$ (Table 3.3). Gly29 is located in the 12-39 Ω-loop structure. The protein structure and the peroxidase activity of the heme proximal mutant of human cyt *c*, in which Thr28, a phosphorylation site, was replaced with Asp (T28D) or Glu (T28E), has been reported[23,24]. Both the T28D and T28E mutants exhibited a peroxidase activity about twice of WT cyt *c*. The results proposed that the introduction of the negative charge near the proximal heme may cause structural change around heme. The introduction of negative charge at position of Gly29, which is closer to heme, caused a structural change that led to improve reactivity with substrates near heme. This idea can be supported by the CD spectra (Figure 3.10B). The CD spectrum of the G29D mutant exhibited two negative bands at 208 and 222 nm (Figure 3.10B). For a globular α-helical protein like cyt *c*, perturbations of the $\theta_{222nm}/\theta_{208nm}$ ratio can be associated with changes in interhelical interactions resulting from changes to the packing of Trp side chains within a protein core[25]. For the G29D mutant, the $\theta_{222nm}/\theta_{208nm}$ ratio is 1.0, smaller than 1.3 determined for WT cyt *c*. Therefore, it has been postulated

that the environment around heme of cyt *c* was perturbed and enhanced flexibility by replacing Gly29 with Asp. Moreover, the $K_{m,RB19}$ of the G29D mutant was greatly reduced compared to WT (Table 3.2). The structural change around heme may also increase the

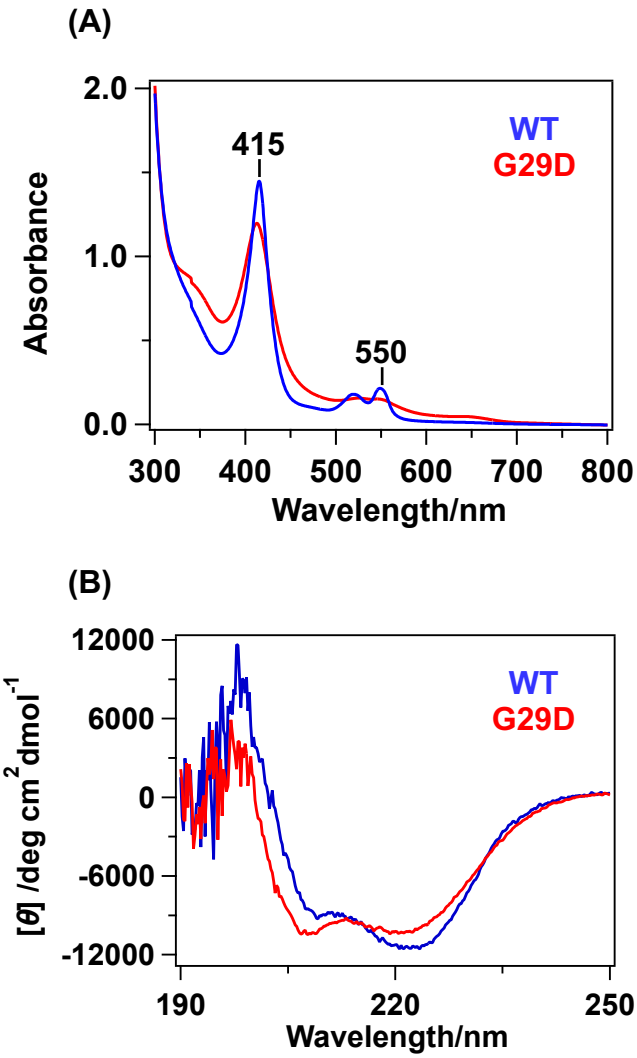

Figure 3.10 (A) Absorbance of supernatant of lysate of *E. coli* expressed WT and G29D cyt *c*. (B) CD spectra of WT and G29D as purified.

accessibility to bulky substrates such as RB19.

The stability of the heme of G29D mutant cyt *c* in *E. coli*

I tried to degrade RB19 using *E. coli* expressing G29D mutant cyt *c* but did not achieve it. Interestingly, *E. coli* pellets expressing this mutant did not show the red color derived from cyt *c* at 24 hours after induction of protein expression (Figure 3.11A and B). This result suggested that the heme of G29D mutant cyt *c* was degraded in cells. To investigate the reason for the ineffectiveness of the G29D mutant as a whole-cell catalyst, transient kinetic spectral changes were monitored using a stopped-flow apparatus to observe the formation of compound I. The absorption spectra of WT cyt *c* in the absence of RB19 were not affected by the reaction with H_2O_2 except for the appearance of a small peak at 550 nm, which would be derived from the formation of ferrous heme (Figure 3.12A). In contrast, the Soret band of the G29D mutant rapidly decreased (Figure 3.12B), indicating that heme was broken by H_2O_2. The absence of absorption at 650–690 nm, characteristic of verdoheme, a well-known intermediate in most heme-degradation reactions, suggests that heme was broken by coupled oxidation. The same reaction was monitored in the presence of RB19. Compared with the spectral changes of WT cyt *c*, the absorbance of RB19 (~595 nm) was largely decreased by the G29D mutant (Figure 3.12C and D). At the same time, the Soret band of the mutant also rapidly decreased. These results indicate that the dye degradation activity of the G29D mutant is much greater than that of WT cyt *c* (Figure 3.12A and B). However, this mutant is not effective as a whole-cell catalyst because heme is easily broken in the reaction with H_2O_2.

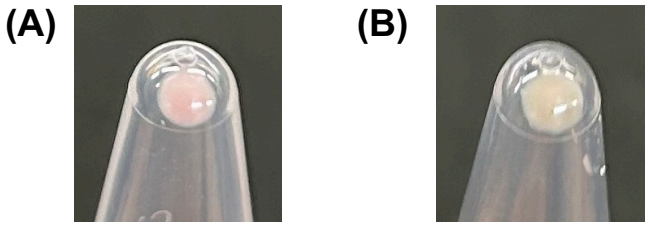

Figure 3.11 Pellets of *E. coli* expressing G29D mutant cyt *c* at (A) 6 h and (B) 24 h after induction of protein expression.

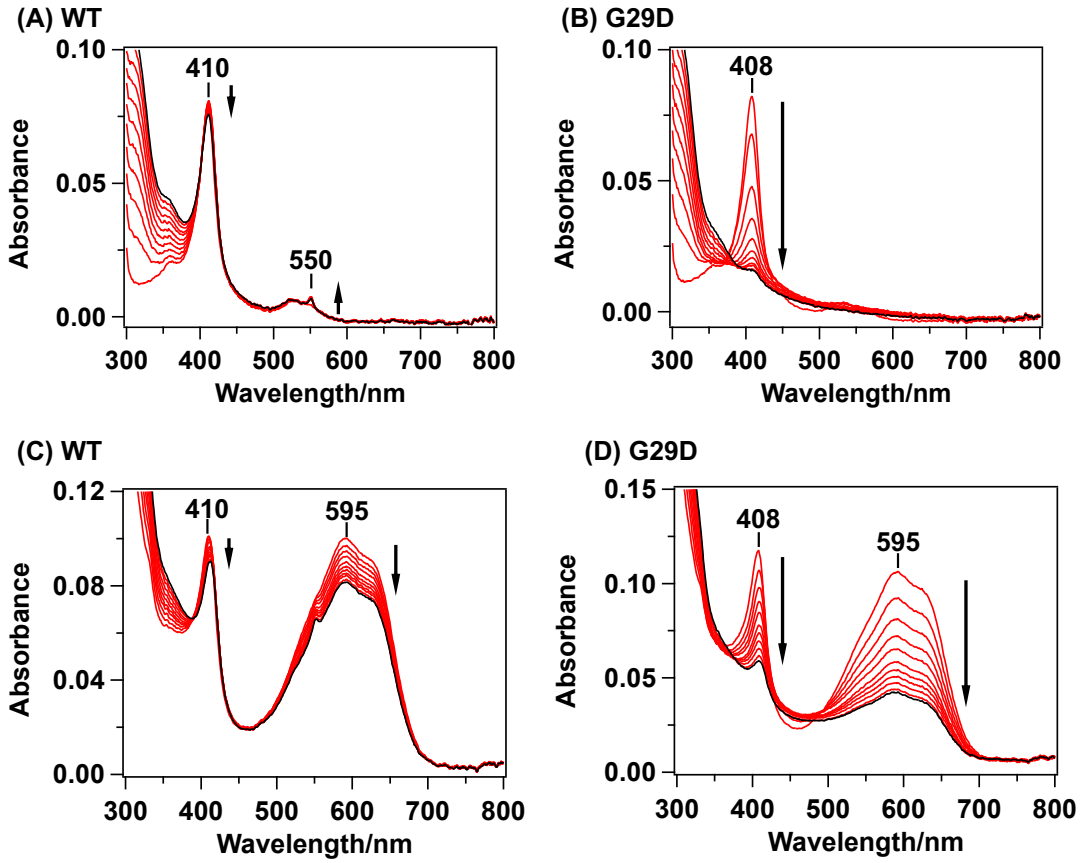

Figure 3.12 Stopped-flow spectra upon mixing (A) WT, (B) G29D (1.0 µM) and H_2O_2 (10 mM); (C) WT, (D) G29D (1.0 µM) and RB19 (40 µM) in the presence of H_2O_2 (10 mM) in sodium phosphate buffer (50 mM, pH 7.0) at 25 °C. Spectra were measured at 6 sec intervals for 60 s.

In summary, I designed several cyt *c* mutants to confer the dye-decolorizing activity. To form a hydrogen bond to axial His, I replaced Gly29 with Asp. The mutation resulted in the drastic enhancement (~80-fold) of the dye-decolorizing activity. The results of a series of mutations indicated that cyt c can be converted into an artificial enzyme that degrades the dye with high efficiency. On the other hand, the heme is easily degraded, which may reduce its activity in the bacteria, indicating the need for further studies, including the search for mutants with enhanced heme stability.

References

1. Belikova, N., Vladimirov, Y., Osipov, A., Kapralov, A., Tyurin, V., Potapovich, M., Basova, L., Peterson, J., Kurnikov, I. & Kagan, V. Peroxidase activity and structuraltransitions of cytochrome c bound to cardiolipin-containing membranes. Biochemistry, **45**, 4998–5009 (2006).
2. Sinibaldi, F., Fiorucci, L., Patriarca, A., Lauceri, R., Ferri, T., Coletta, M. & Santucci, R. Insights into cytochrome c-cardiolipin interaction. Role played by ionic strength. Biochemistry, **47**, 6928–6935 (2008).
3. Pollock, W., Rosell, F., Twitchett, M., Dumont, M. & Mauk, A. Bacterial expression of a mitochondrial cytochrome c. Trimethylation of Lys72 in yeast iso-1-cytochrome C and the alkaline conformational transition. Biochemistry, **37**, 6124–6131 (1998).
4. Jeng, W., Chen, C., Chang, H. & Chuang, W. Expression and Characterization of Recombinant Human Cytochrome c in E. coli. J. Bioenerg. Biomembr., **34**, 423–431 (2002).
5. Beers, R. & Sizer, I. A spectrophotometric method for measuring the breakdown of hydrogen peroxide by catalase. J. Biol. Chem., **195**, 133–140 (1952).
6. Wang, Z. Lin, Y., Rosell, F., Ni, F., Lu, H., Yang, P., Tan, X., Li, X., Huang, Z., & Mauk A. Converting cytochrome c into a peroxidase-like metalloenzyme by molecular design. ChemBioChem, **8**, 607–609 (2007).
7. Cervelli, M., Mariottini, P., Smulevich, G., Coletta, M. & Fiorucci, L. The Met80Ala and Tyr67His/Met80Ala mutants of human cytochrome c shed light on the reciprocal role of Met80 and Tyr67 in regulating ligand access into the heme pocket. J. Inorg. Biochem., **169**, 86–96 (2017).
8. Savenkova, M., Kuo, J. & Ortiz de Montellano, P. Improvement of peroxygenase activity by relocation of a catalytic histidine within the active site of horseradish peroxidase. Biochemistry, **37**, 10828–10836 (1998).
9. Zhang, P., Xu, J., Wang, X., He, B., Gao, S. & Lin, Y. The Third Generation of Artificial Dye-Decolorizing Peroxidase Rationally Designed in Myoglobin. ACS Catal., **9**, 7888–7893 (2019)..
10. Uchida, T., Sasaki, M., Tanaka, Y. & Ishimori, K. A Dye-Decolorizing Peroxidase from Vibrio cholerae. Biochemistry, **54**, 6610–6621 (2015).
11. Strittmatter, E., Liers, C., Ullrich, R., Wachter, S., Hofrichter, M., Plattner, D. & Piontek, K. First crystal structure of a fungal high-redox potential dye-decolorizing peroxidase substrate interaction sites and long-range electron transfer. J. Biol. Chem., **288**, 4095–4102 (2013).

12. Linde, D. Pogni, R., Cañellas, M., Lucas, F., Guallar, V., Baratto, M., Sinicropi, A., Sáez-Jiménez, V., Coscolin, C., Romero, A., Medrano, F., Ruiz-Dueñ;as, F. & Martínez, A. Catalytic surface radical in dye-decolorizing peroxidase: A computational, spectroscopic and site-directed mutagenesis study. Biochem. J., **466**, 253–262 (2015).
13. Shrestha, R., Chen, X., Ramyar, K., Hayati, Z., Carlson, E., Bossmann, S., Song, L., Geisbrecht, B. & Li, P. Identification of surface-Exposed protein radicals and a substrate oxidation site in a-Class dye-Decolorizing peroxidase from thermomonospora curvata. ACS Catal., **6**, 8036–8047 (2016).
14. Chaplin, A., Wilson, M. & Worrall, J. Kinetic characterisation of a dye decolourising peroxidase from Streptomyces lividans: New insight into the mechanism of anthraquinone dye decolourisation. Dalton Trans., **46**, 9420–9429 (2017).
15. Bushnell, G., Louie, G. & Brayer, G. High-resolution three-dimensional structure of horse heart cytochrome c. J. Mol. Biol., **214**, 585–595 (1990).
16. Finzel, B., Poulos, T. & Kraut, J. Crystal structure of yeast cytochrome c peroxidase refined at 1.7-Å resolution. J. Biol. Chem, **259**, 13027–13036 (1984).
17. Hannibal, L., Tomasina, F., Capdevila, D., Demicheli, V., Tórtora,V., Alvarez-Paggi, D., Jemmerson, R., Murgida, D., & Radi, R. Alternative Conformations of Cytochrome c: Structure, Function, and Detection. Biochemistry, **55**, 407–428 (2016).
18. Sinibaldi, F., Howes, B., Piro, M., Caroppi, P., Mei, G., Ascoli, F., Smulevich, V., & Santucci, R. Insights into the role of the histidines in the structure and stability of cytochrome c. J. Biol. Inorg. Chem., **11**, 52–62 (2006)
19. Torres, E., Victor Sandoval, J., Rosell, F., Grant Mauk, A. & Vazquez-Duhalt, R. Site-directed mutagenesis improves the biocatalytic activity of iso-1-cytochrome c in polycyclic hydrocarbon oxidation. Enzyme Microb. Technol., **17**, 1014–1020 (1995).
20. Rafferty, S., Smith, M. & Mauk, A. Azide binding and active site dynamics of position-82 variants of ferricytochrome c. Inorg. Chim. Acta, **242**, 171–177 (1996).
21. Lei, H., Nold, S., Motta, L. & Bowler, B. Effect of V83G and i81A substitutions to human cytochrome c on acid unfolding and peroxidase activity below a neutral pH. Biochemistry, **58**, 2921–2933 (2019).
22. Samsri, S., Prasertsuk, P., Nutho, B. & Pornsuwan, S. Molecular insights on the conformational dynamics of a P76C mutant of human cytochrome c and the enhancement on its peroxidase activity. Arch. Biochem. Biophys., **716**, 109112

(2022).
23. Guerra-Castellano, A., Díaz-Moreno, I., Velázquez-Campoy, A., De La Rosa, M. A. & Díaz-Quintana, A. Structural and functional characterization of phosphomimetic mutants of cytochrome c at threonine 28 and serine 47. Biochim. Biophys. Acta. Bioenerg., **1857**, 387–395 (2016).
24. Mahapatra, G. Mahapatra, G., Varughese, A., Ji, Q., Lee, I., Liu, J., Vaishnav, A., Sinkler, C., Kapralov, A., Moraes, C., Sanderson, T., Stemmler, T., Grossman, L., Kagan, V., Brunzelle, J., Salomon, A., Edwards, B., & Hüttemann, M. Phosphorylation of cytochrome c threonine 28 regulates electron transport chain activity in kidney: Implications for amp kinase. J. Biol. Chem., **292**, 64–79 (2017).
25. Arnold, G., Day, L. & Keith Dunker, A. Tryptophan Contributions to the Unusual Circular Dichroism of fd Bacteriophage. Biochemistry, **31**, 7948–7956 (1992).

CHAPTER IV

Conclusions

DyPs can degrade persistent dyes, so they have potential application for bioremediation. However, its low optimal pH of the activity hinders the industrial use of DyP, and increasing activity under neutral conditions is required. In the present thesis, I aimed to rationally design an artificial enzyme with persistent dye-degrading activity that can be used for environmental purification. The results and conclusions drawn from experimental data are summarized below.

1. pH-dependence of dye-degrading activity of DyP

To shift the optimal pH of dye-degrading activity of *Vc*DyP, I identified the key factor for pH-dependence of the activity. Replacing Asp138 with Val led to a shift in the optimal pH to 6.5 and exhibited 9-fold higher specific activity that of WT *Vc*DyP at pH 7. I proposed that the hydrogen bond between Asp138 and His178 plays a key role in the pH dependence of dye-decolorizing activity of *Vc*DyP. The introduction of a mutation that inhibits the hydrogen bonding may have fixed the orientation of the side chain of His178, which may have led to the transfer of radicals to the substrate binding site in the neutral region, resulting in the increased dye-degrading activity of DyP in the neutral region. In conclusion, by introducing mutations based on the reaction mechanism, I succeeded for the first time in the rational design and creation of a mutant DyP with a neutral pH optimum for dye-degrading activity.

2. Converting cytochrome *c* into a DyP-like enzyme

E. coli expressing D138V mutant *Vc*DyP had a low RB19 degrading activity due to the absence of heme-bound enzymes. In order to create the artificial enzyme which can degrade RB19 in cells, I constructed cyt *c* mutants based on the structural information of peroxidases and DyPs. Mutational studies showed that introducing Asp into the proximal heme decreased K_m of dye-degrading activity and enhanced 80-fold catalytic efficiency. In addition, the dye-degrading activity of WT cyt *c* required a high concentration of H_2O_2, 20 mM, while that of G29D mutant cyt *c* proceeded at 0.2 mM H_2O_2, like that of *Vc*DyP, and exhibited a higher specific activity at pH 8.5 than that of D138V mutant *Vc*DyP at pH 6.5 (Figure 4.1). These results provide a new perspective for the future design of artificial DyP.

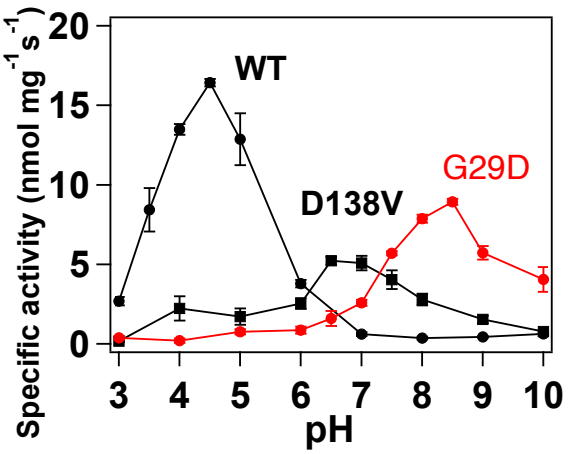

Figure 4.1 pH profiles of RB19-decolorizing activities of WT *Vc*DyP (black circle), D138V mutant *Vc*DyP (black square), and G29D mutant cyt *c* (orange). The reaction was initiated by the addition of proteins (0.3 μM) to RB19 (40 μM) in the presence of H_2O_2 (0.2 mM) at 25 °C.

Conclusion remarks

In conclusion, I demonstrated that a highly active dye-degrading enzyme can be created by rational design using DyP, whose structure and dye-degrading reaction mechanism are already known. However, these mutants have low intracellular heme binding and heme stability, making their use as whole-cell biocatalyst difficult. Several studies have focused on improving the thermal stability and reusability of enzymes by immobilizing them on mesoporous materials[1–3], amino-functionalized nanosilica[4,5] . In the future, not only to explore mutants having high dye-degrading activity and high protein stability, but also to examine the immobilization of enzymes on polymeric materials such as mesoporous materials will be expected to lead to the creation of new treatment technologies for effluents containing synthetic dyes, using enzymes.

References

1. El-Nahass, M. N., El-keiy, M. M. & Ali, E. M. M. Immobilization of horseradish peroxidase into cubic mesoporous silicate, SBA-16 with high activity and enhanced stability. Int. J. Biol. Macromol., **116**, 1304–1309 (2018).
2. Shakeri, M. & Shoda, M. Decolorization of an anthraquinone dye by the recombinant dye-decolorizing peroxidase (rDyP) immobilized on mesoporous materials. J. Mol. Catal. B. Enzym., **54**, 42–49 (2008).
3. Shakeri, M. & Shoda, M. Efficient decolorization of an anthraquinone dye by recombinant dye-decolorizing peroxidase (rDyP) immobilized in silica-based mesocellular foam. J. Mol. Catal. B. Enzym., **62**, 277–281 (2010).
4. Gahlout, M., Rudakiya, D. M., Gupte, S. & Gupte, A. Laccase-conjugated amino-functionalized nanosilica for efficient degradation of Reactive Violet 1 dye. Int. Nano Lett., **7**, 195–208 (2017).
5. Yang, F. Backov, R., Blin, J., Fáklya, B., Tron, T., Mekmouche, Y. Site directed confinement of laccases in a porous scaffold towards robustness and selectivity. Biotechnol. Rep., **31**, (2021).